Geophys. J. Int. (1993) **115**, 1095–1118

A quantitative methodology to extract regional magnetotelluric impedances and determine the dimension of the conductivity structure

R. W. Groom,* R. D. Kurtz, A. G. Jones and D. E. Boerner
Geological Survey of Canada, 1 Observatory Crescent, Ottawa, Ontario, K1A 0Y3, *Canada*

Accepted 1993 May 24. Received 1993 May 21; in original form 1992 May 11

SUMMARY

A methodology to determine quantitatively the dimensionality of the dominant conducting structures and the resolution of the structural parameters in magnetotelluric data is presented. In addition, the method recovers the regional impedance responses when the regional structure can be characterized, at least approximately, as 1- or 2-D. The methodology is based upon three general models of the MT tensor, each of which has a distinct parameterization and physical interpretation. A weighted statistical residual describes quantitatively the fit of the model response to the data within the scatter of the measured data and hence permits: (1) tests of dimensionality, (2) determination of the appropriate strike angle, and (3) recovery of the regional responses.

The method has been tested extensively with synthetic data and proven to be successful. These synthetic studies give insight into the different physical parameterizations and the stability of the parameters determined. We describe and illustrate some of these synthetic studies. With field data, the methodology is not always as straightforward, but its application to a great many sites has proven valuable. Data from two closely spaced sites, which are both affected by strong but very different 3-D effects, are analysed to illustrate the geological significance of the results. The analyses reveal and recover regional responses within the data which indicate the presence of electrical anisotropy located deep in the crust and upper mantle. Analyses of the entire data set, of which these two form a part, confirm this finding.

Key words: decomposition, galvanic distortion, magnetotelluric data analysis, structural dimensionality.

INTRODUCTION

With the increased sophistication of acquistion, processing and interpretation schemes for magnetotelluric (MT) data, the ability to quantify the dimensionality of the dominant conductivity structure becomes increasingly important. For example, one must determine if the structure is significantly 3-D within the errors of the data, and to what extent this three-dimensionality may affect the validity of 1-D or 2-D models of the MT responses. Due to the significance of near-surface effects, investigators often rotate their data into an assumed geo-electric strike coordinate system, and then model either one or both of the off-diagonal elements of the rotated tensor in an attempt to derive the regional or large-scale structure. It is therefore critical to determine the extent to which the data actually fit dimensionality assumptions, prior to modelling and geological interpretation.

Determining the characteristics of the conductivity structure implied by broad-band MT data is not trivial, and has been the subject of much study during the last decade. The effective extent and penetration depth of the electromagnetic fields increase with period, which implies that the apparent dimensionality of the conductivity structure will, in general, be frequency dependent. Regional strike directions and apparent dimensionality can change when a conductive structure, which may be approximately 2-D at short periods, becomes fully 3-D at longer periods

*Now at: Department of Geological Sciences, Queen's University, Kingston, Ontario K7L 3B6, Canada.

(see, e.g. Jones 1983). At these periods, where the response of the large structure can no longer be approximated by a 2-D model, it may have both frequency-independent (*static*) effects, as well as significant frequency-dependent effects caused by induction or by the magnetic effects of current channelling. Eventually, at even longer periods, the structure will become simply a *static* distorting structure. The effective dimensionality, as a function of period, is clearly required prior to modelling or inversion of data containing different physical responses.

The method proposed here can be applicable to all data since at some period, and longer, the problem of small-scale electric scattering cannot be avoided, as the period of oscillation affects the physical *scale* length of the entire experiment, including the recording system. At long periods and large skin depths, even extended electric-field measurements with electrode lengths of a few kilometres can be essentially point measurements when the significant 3-D structures have scale lengths of tens of kilometres or more. Thus, the analyses proposed here are applicable also to EMAP (Torres-Verdin & Bostick 1992) and grid-type surveys when the periods of interest are long enough such that the appropriate skin depths become comparable with, or larger than, the spatial sampling or averaging windows.

We first describe three physically based decompositions of the MT tensor; a simple 1-D model (Cagniard 1953), the conventional 2-D model (Swift 1967), and a 3-D parameterization (Groom & Bailey 1989). A χ^2 misfit statistic is defined for use in quantifying the simplest, yet appropriate model. With the use of synthetic 2-D and 3-D data, we illustrate an analytic approach for examining MT data using the three decompositions and the misfit statistic. The analyses include the use of graphical representations of parameter stability, resolution and decomposition model fits of the data.

3-D scattering effects often cause significant shifts in the amplitude of apparent resistivity curves. Even 3-D decompositions suffer from these effects (Groom & Bahr 1992). The nature, magnitude and means for correcting these shifts are investigated, including the introduction of a new 1-D estimator which offers some improvement over the conventional determinant (*effective*) and anti-trace (*average*) impedance estimators (Berdichevsky & Dmitriev 1976).

Recovery of lower dimensional regional (i.e. large scale) responses from 3-D data has many problems. Some of these problems, and the ability to recover these responses with the described methodology, are examined with the use of data from two relatively close (separated by 15 km) sites, which suffer from quite different 3-D scattering effects. The two sites are part of a much larger data set covering several hundred kilometres, all of which have been analysed with the suggested method. Prior to this process, the data were difficult to interpret using conventional tools, as they varied dramatically over short distances and gave regional impedance responses which appeared physically implausible.

PHYSICAL MODELS FOR IMPEDANCE TENSOR

The simplest model of the earth is a layered or 1-D model where the impedance tensor is simply estimated by the expression;

$$\bar{\bar{\mathbf{Z}}}(\omega) = \begin{bmatrix} 0 & Z_0(\omega) \\ -Z_0(\omega) & 0 \end{bmatrix}. \tag{1}$$

In this case, there is a single complex impedance $Z_0(\omega)$ and thus there are only two model parameters per frequency, namely the magnitude and complex phase of Z_0 (Cagniard 1953). As well, one might wish to impose smoothing or causality constraints on model parameters, thus reducing the number of parameters required over the entire frequency range.

A somewhat more complicated and extensively used model is to assume a 2-D structure with conductivity varying both vertically and in one lateral direction. In the absence of noise, the MT data tensor is estimated by:

$$\bar{\bar{\mathbf{Z}}}(\omega) = \mathbf{R}(\theta)\begin{bmatrix} 0 & Z_{\parallel}(\omega) \\ -Z_{\perp}(\omega) & 0 \end{bmatrix}\mathbf{R}^{\mathrm{T}}(\theta) \tag{2}$$

where $\mathbf{R}$ is a rotation operator. $Z_{\parallel}$ is the impedance associated with the Transverse Electric (TE) mode while $Z_{\perp}$ is the impedance of the Transverse Magnetic (TM) mode. There are five parameters per frequency (Swift 1967) for this model although it is possible (and even desirable) to impose constraints on the regional strike θ by requiring it, for example, to be frequency independent.

It is also possible to have a 3-D parameterization to represent the galvanic effects of small-scale conductive structure. If the frequency is sufficiently low that the 3-D structure has a negligible inductive response, and the incident field due to the regional structure and neighbouring small-scale structures is sufficiently uniform, then the EM fields can be described, to first order, by galvanic distortion or scattering of regional (1-D or 2-D) electric fields while the regional magnetic field remains unchanged (Bahr 1988; Groom & Bahr 1992). Thus the impedance tensor is estimated by

$$\bar{\bar{\mathbf{Z}}}(\omega) = \mathbf{R}(\theta)\mathbf{C}(\theta)\begin{bmatrix} 0 & Z_{\parallel}(\omega) \\ -Z_{\perp}(\omega) & 0 \end{bmatrix}\mathbf{R}^{\mathrm{T}}(\theta) \tag{3a}$$

where $\mathbf{C}(\theta)$ is the 3-D galvanic electric scattering or distortion operator represented in the regional 2-D co-ordinate frame (Zhang, Roberts & Pedersen 1987; Bahr 1988; Groom & Bailey 1989). This model has up to nine parameters per frequency although all are not necessarily independent or determinable. There are a number of methods for decomposing the impedance tensor under this physical model (Larsen 1977; Zhang *et al.* 1987; Bahr 1988; Groom & Bailey 1989; Chakridi, Chouteau & Mareschal 1992). The basic conclusions and limitations of these methods will be quite similar although the specific details of actual application have yet to be fully compared (Groom & Bahr 1992).

It is possible, with techniques of Groom & Bailey (1989, 1991; hereafter termed GB1 and GB2), to decompose the data under this 3-D galvanic distortion model to obtain, in general, seven uniquely determined parameters per frequency; namely the regional 2-D strike θ, two parameters partially describing the effects of the local electric field distortion ('twist' and 'shear'), and the 2-D complex regional impedances ($Z_{\parallel}$, $Z_{\perp}$). The true regional 2-D impedances can be scaled by two real numbers defined

by GB1 as a local anisotropy **A** and site gain g, so that

$$\bar{\bar{\mathbf{Z}}}(\omega) = \mathbf{R}(\theta)\mathbf{TS}\left\{g\mathbf{A}\begin{bmatrix} 0 & Z_{\parallel}(\omega) \\ -Z_{\perp}(\omega) & 0 \end{bmatrix}\right\}\mathbf{R}^{\mathrm{T}}(\theta) \tag{3b}$$

providing eight non-linear real equations in seven real unknowns. The anti-symmetric operator, **T**, and the symmetric operator, **S**, are termed twist and shear respectively. The diagonal operator, **A**, is an anisotropy operator, while the scalar, g, is termed the site gain. It may be desirable, depending upon the characteristics of the data, to constrain the distortion parameters as well as the regional strike to be independent of frequency over all, or some subset, of the frequency bandwidth.

The models (1)–(3) obviously do not include all effects of all possible conductivity structures at any arbitrary period. However, even though more complicated physical models can be envisaged, it may not be possible to extract the parameters from the data (Bahr 1991). Accounting for the magnetic field response of 3-D galvanic scattering is one additional complexity which can be qualitatively accounted for (GB2; Groom 1988; Jones & Groom 1993). It is arguable that, except for certain types of extremely large structures, both the inductive and galvanic magnetic effects are secondary (save for a very narrow frequency band) to those included in models 1–3 (GB2; Groom & Bahr 1992). Thus, if none of the three models adequately fits the data then this places strong constraints on the conductivity structure.

QUANTITATIVE TESTING FOR DIMENSION AND STRUCTURAL PARAMETERS

An important aspect of applying the physical models (1)–(3) to real data is the computation of some measure of misfit to appraise quantitatively the appropriateness of the model. Having modelled the data to one of the three physical hypotheses and obtained the model parameters (possibly constrained), the model hypothesis is tested with a χ^2-like misfit variable. This is a residual error for the fit of the model to the data, normalized by estimates for the variance (σ_{ij}^2) of each element of the tensor data:

$$\gamma^2 = \tfrac{1}{4}\sum_{i=1}^{2}\sum_{j=1}^{2}\frac{|\hat{Z}_{ij} - Z_{ij}|^2}{\sigma_{ij}^2} \tag{4}$$

where Z_{ij} and $\hat{Z}_{ij}$ are the modelled and measured tensor elements, respectively. The variances would usually be estimated from the sample population of tensor estimates. However, often the variances are those of the mean impedance estimates. In practice, the data are fit to a model (1)–(3) by minimizing a functional which is defined by an L2 norm. The statistical meaning of this minimization is then examined by the use of the χ^2 norm (4).

If the errors in the mean impedance estimates are distributed randomly, and we require the modelled tensor elements to be fit almost always with two standard deviations of the data, then the misfit γ^2 would be expected to lie within the range 0–4. If none of the three models fit within these levels, this could imply that not all physical effects have been included (i.e. 3-D induction). The residual γ^2 emphasizes the fit of the model elements to the corresponding data elements which have the smallest variance. However, if the variances are poorly estimated then this statistic (4) may be biased either up or down. In this case, we might seek the model with the lowest residual statistic. A graphical display of the fit of the impedance tensor to a particular parameterization has proven most useful since the γ^2 statistic can vary significantly between adjacent periods due to either the randomness of the noise or poor variance estimates (e.g. Figs 2b, 3b, 15b and 16b).

The *best* model is not necessarily the one with the lowest average residual (averaged over periods) because there is always a trade-off between minimizing residual and maximizing smoothness. By smoothness (by analogy to polynomial line fitting), we mean the fewest number of parameters used over a data set (i.e. a set of frequencies or a set of stations or both). For example, under model (3) if the strike and the distortion parameters (twist and shear) are all constrained to be a constant over N frequencies, then we will have used $4N+3$ independent parameters for N frequencies. On the other hand, if model (2) is used and strike is not constrained to be independent of frequency, we will have used $5N$ parameters and if $N>3$ we have a rougher model. We could, of course, include additional constraints to smooth the model such as requiring the impedances to vary smoothly with period (i.e. fit to an m-order polynomial). The increase in the residual associated with any smoothing must be appraised to assess if the response of the constrained model is representative of the observed data. Implicit in this process is an assumption of the nature of the scattering process. If, for example, different scattering processes become significant as the frequency decreases (due possibly to multiple scatterers) then some smooth transition of distortion parameters may occur.

AN EXAMPLE WITH SYNTHETIC DATA

The methodology and associated graphical analyses techniques can be demonstrated by studying 3-D synthetic impedance data which are generated by superposing 2-D numerical and 3-D analytic responses (GB2). The model comprises a 3-D homogeneous hemisphere embedded in a 2-D regional structure (Fig. 1), and is described in detail in GB2. The hemisphere is sufficiently small for the frequencies used here that it has a negligible inductive response (GB2). However, the conductivity contrast between the hemisphere and the host produces a charge distribution which has significant effects upon both the electric and magnetic fields. The non-inductive effects of the hemisphere on the fields produced by the large-scale 2-D structure can be expressed via scattering operators described in GB2. The resulting impedance data can then be rotated to any desired coordinate system to represent a given *measurement* system. For this illustration, Gaussian noise was added such that the variance of the noise is identical for all four elements of the tensor.

Consider the 2-D regional MT response at the site of the hemisphere (i.e. ignoring the response of the hemisphere) where the measurement co-ordinate system is taken to be 30° counter-clockwise to strike and with 3 per cent noise added. We parameterize this data under model (2) to illustrate a few aspect of the analyses presentation. Figs 2(a) and (b) contain the best fitting parameters of model (2) with

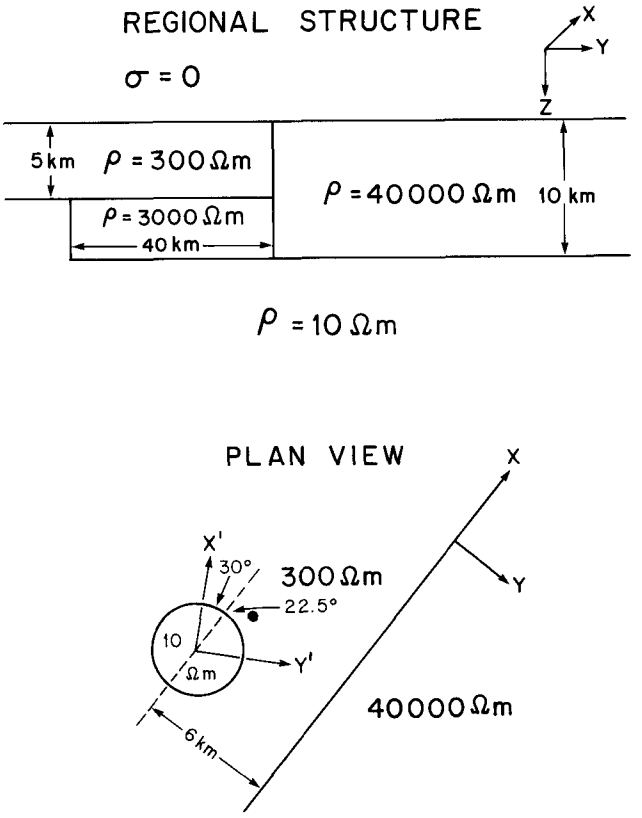

Figure 1. The synthetic regional 2-D conductivity structure (GB2) not to scale. The measurement site is indicated. The hemisphere has a 50 m radius and is located 6 km from the vertical contact in the 2-D model. The measurement axes labelled x' and y' are rotated 30° anticlockwise from the 2-D intrinsic co-ordinate system (strike based).

no constraints and the resulting fit to the data. Fig. 2(a) contains the traditional 2-D regional apparent resistivity [iii] and phase [iv] estimates in the resulting strike-coordinate frame. The convention used here is to remove the negative from the yx-components of the regional impedance estimate. Thus for a 1-D response, the phases will be equal. Fig. 2(a)[i] contains the logarithm of the statistical residual (4) for this model. Note that the chi-square variable has, as expected, a value generally less than 4 (line on figure). Fig. 2(a)[ii] illustrates the strike estimates and the traditional skew as an angle (i.e. $\tan^{-1}$[skew]). For periods less than 0.1 s, the strike azimuth is poorly defined as the skin depth is small and the model appears 1-D. The ability to determine such a weakly defined strike is dependent upon the amount of noise in the data. At long periods, there is little to differentiate the phases of the two modes and the apparent resistivities are parallel. In effect, the 2-D structure has become essentially a thin sheet with primarily a galvanic-type response.

The scatter in a parameter, as indicated by the error bars in Fig. 2(a), is determined empirically because the parameters generally are not linearly dependent upon the noise. Realizations of the noise are generated randomly using the given noise statistics and are added to the mean tensor estimate. (This can be done for both synthetic or experimental data.) Each realization of the mean impedance tensor is then fit to the particular decomposition model with possible constraints. The scatter in a parameter is determined from the spread of the parameter estimates with the set of realizations and then displayed as an error bar. In a non-linear system, such as here, noise will generally tend to bias a parameter estimate rather than scatter it uniformly about a mean. Thus, it is possible that the parameter derived from mean tensor data will have a value that does

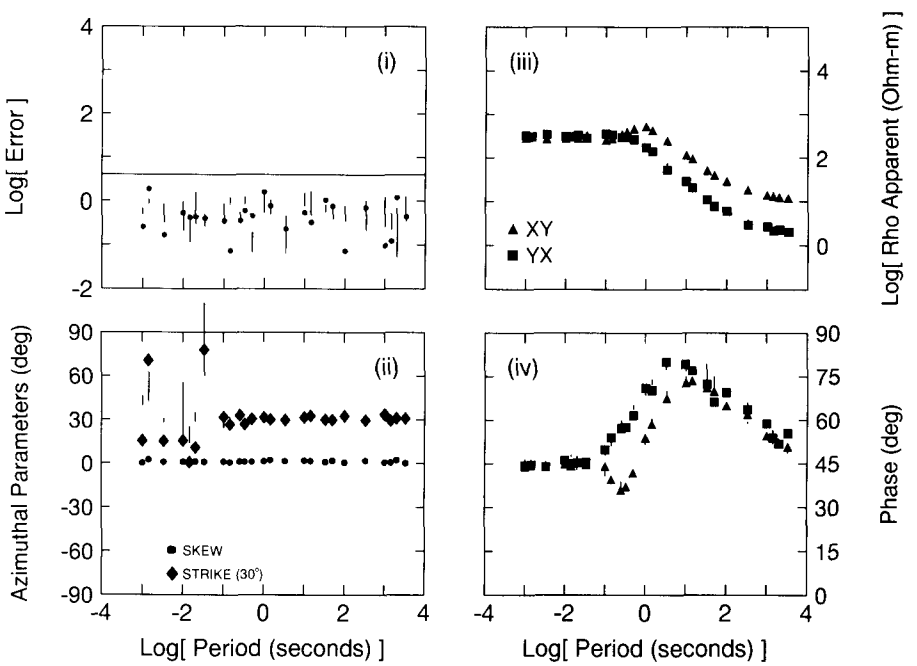

Figure 2(a). Standard parameter display. (i) Residual error of the fit of the model to the data, (ii) azimuthal parameters (strike and skew), (iii) estimated regional apparent resistivities in strike azimuth, (iv) estimated regional phases. The parameters are calculated for 2-D synthetic data (including 3 per cent noise), which were rotated to the measurement system. The values given at the bottom of the 'Azimuthal Parameters' plot are the average values for these parameters over the entire period band.

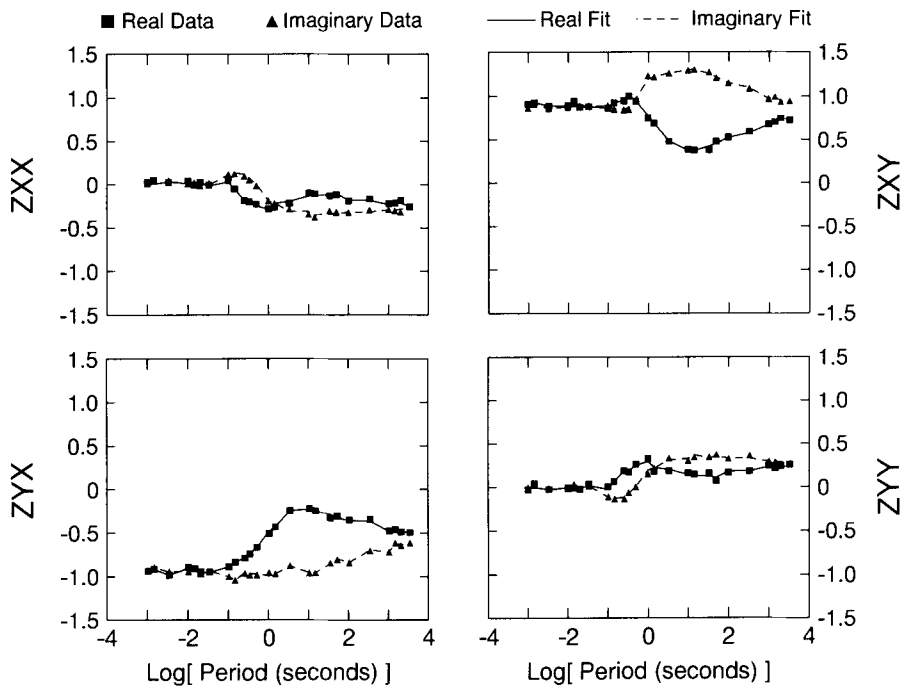

Figure 2(b). Fit of the model parameterization of Fig. 2(a) to the scaled impedance data (see text for details). Error bars indicate one standard deviation of the data. Square symbols and solid lines represent in-phase data and model impedance. Triangular symbols and dashed lines represent quadrature data and model impedance.

not fall within the error bars of the realizations when the data variance is large. (Fig. 2a.)

Figure 2(b) displays, by impedance element, the fit of the measured data (in the measurement co-ordinate system) to the response associated with the model parameters of Fig. 2(a). The data and the estimated impedance tensor have both been scaled by the impedance of a layer over a half-space model, which allows the scaled data with the model fit to be plotted over the entire spectrum on a linear-amplitude scale for each visual comparison. The data are plotted as symbols with error bars while the fit to the data (*estimated impedances*) are given as either solid (*real*) or dotted (*imaginary*) lines. The fit is presented in the measurement coordinate frame for simplicity. Displaying the fit in a rotated coordinate frame would require obtaining estimates of the impedance errors in that coordinate frame. Obtaining the errors in the rotated frame from the original errors requires strong restrictions on the statistical distribution of the errors in the measured fields and on the covariance distributions between the fields. Of course, recalculation of the errors in the coordinate frame could be accomplished by rotating the original time series or Fourier spectra and rederiving the impedance estimates from recalculated cross-spectral estimates.

Consider a 3-D test site located 16 m outside the hemisphere at an angle of 22.5° clockwise to strike (Fig. 1). The data measurement axes are as above (30°CCW from strike). Figs 3(a) and (b) display the parameterization information for the impedance model (2) and the fit to the data. An unrealistically low noise level (0.1 per cent) was added initially to demonstrate several points. At the highest frequencies, the skew is near zero (Fig. 3) but increases as the fields become increasingly more sensitive to the 2-D structure. (This effect is due to the symmetry of the 3-D body and site location.) The strike angle is approximately 52.5° at the short periods (the azimuthal position of the site relative to the measurement axes) and decreases to a long-period azimuth of about 45°. At high frequencies, the regional structure is 1-D and thus the current polarization is defined entirely by the local structure. For this isometric structure it is easily determined that the local current is polarized along a radial axis given by the azimuthal location of the site. At long periods, the polarization angle of the current is determined both by the 3-D current channelling and the current pattern of the 2-D structure. These aspects are discussed more fully in GB2.

The impedance phase plot (Fig. 3(a)[iv]) shows that the general nature of the regional phase response is recovered (compare with Fig. 2(a)[iv]). However, at the shortest periods, small effects on the phase by the current distortion (GB2) can be seen. The apparent resistivities (Fig. 3(a)[iii]) are shifted and there are small changes in shape from the regional responses. In the residual plot (Fig. 3(a)[i]), we see that the error rises from an acceptable misfit over the first two decades to a misfit greater than 100 at the longest periods. The 2-D parameterization actually fits the high-frequency data which is essentially caused by 3-D scattering of a 1-D regional response. This is due to the symmetry of the hemisphere which results in a 3-D electric scattering matrix that is symmetric and thus can be diagonalized. Therefore, the resulting impedance tensor can be anti-diagonalized if the regional data is 1-D since the 1-D impedance tensor commutes with the rotation operator. This symmetry also explains a skew of zero for the high frequencies. Fig. 3(b) shows the 2-D decomposition fit to the data. The effects of the 3-D body and the attempt to fit a

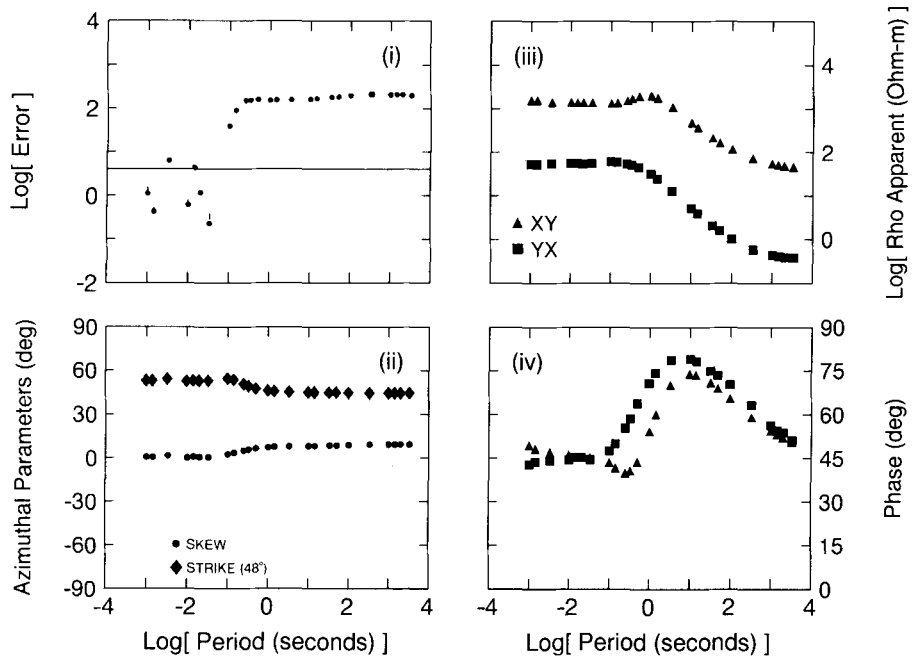

Figure 3(a). The residual error (i), strike, skew (ii), and regional apparent resistivity and phase (iii, iv) estimates for a 2-D model parameterization of the synthetic 3-D data with 0.1 per cent noise.

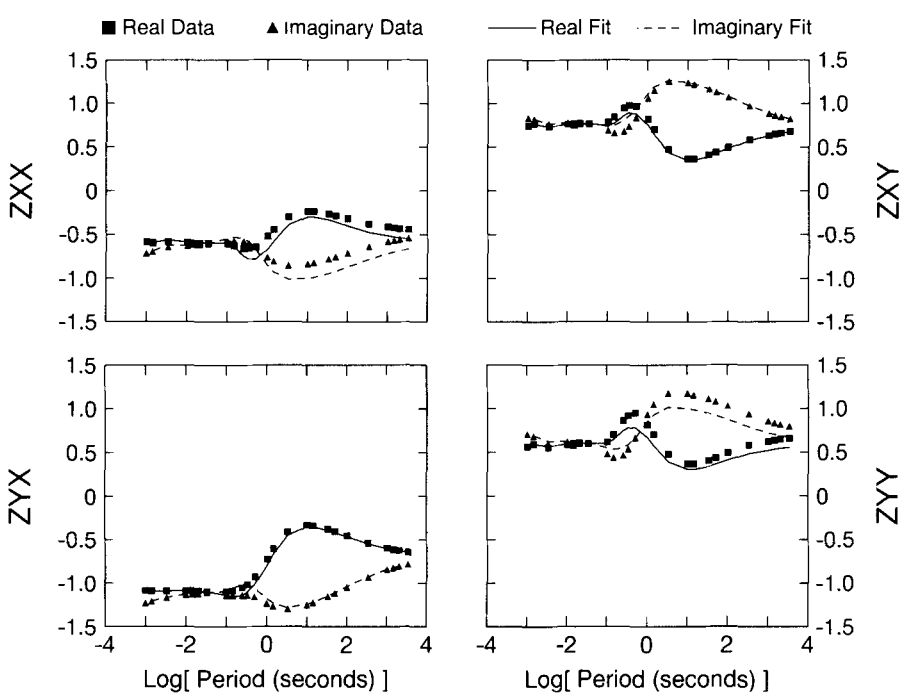

Figure 3(b). Parameterization fit to scaled data.

2-D model, can be seen clearly by comparing Figs 2(b) and 3(b). The off-diagonal elements are generally well fit (in accordance with the mathematics of this decomposition) while the diagonal elements are poorly fit at the longer periods.

Figure 4 shows the parameterization for model (2) for the same data with the noise contribution increased to 2 per cent. The larger noise level results in a minor impedance phase which is essentially undetermined. However, the strike estimation is similar to, but not as smooth as, the low-noise case. The 2-D strike estimate from data with relatively strong current channelling effects is actually an estimate of the local current azimuth (GB2). The long-period residual (Fig. 4[i]) has now dropped an order of

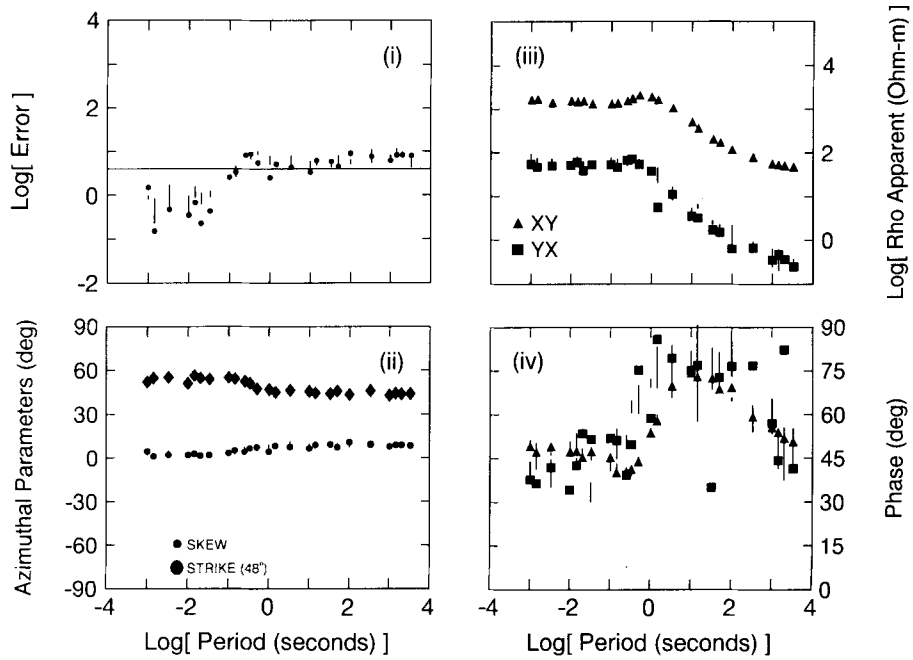

Figure 4. The residual error, strike, skew, regional impedance estimates for a 2-D model parameterization of 3-D data with 2 per cent noise.

magnitude, compared to the lower noise case (Fig. 3(a)[i]), to near 10 due to the increased variance of the data estimates. Although this is at the limit of an acceptable value, the consistency of the value, from period to period, indicates a 3-D model is still most probable.

Applying parameterization model (3) to the 3-D synthetic data set, Fig. 5 displays some of the 3-D parameters for the low noise (0.1 per cent) data set. The figure presents the γ^2 residual, a normalized error, the twist, shear and channelling parameters as functions of period and 2-D rotation angle (i.e. assumed strike). The parameters and residual information for the plot are obtained by constraining the strike at increments of 3° from 0–90° and then recovering the remaining parameters of the GB1 3-D decomposition as functions of this constrained strike.

Two residual error plots are given. The first is the logarithm to base 10 of γ^2 (4). If the noise were distributed normally with a given variance, a logarithmic value of 0.3 would represent approximately 1.41σ ($\approx$85 per cent). Thus a blue to blue-green shaded γ^2 indicates a good fit. (Note the asymmetry in the contoured error.) Although the correct strike (30°) is well determined in the mid-to-long periods, both the shortest and longest periods show only weak preference for this azimuth. At the shortest periods, the data are not sensitive to the 2-D contact, whereas at the longest periods the 2-D structure is inductively thin and has essentially no phase response (the 2-D TE and TM impedances have almost the same phase although different magnitudes). At these long periods, the 2-D impedance tensor can be approximately described by a 2-D real distortion matrix operating on a 1-D complex impedance tensor, i.e.

$$\bar{\bar{\mathbf{Z}}}_{2\text{-D}}(\omega) \approx \mathbf{R}(\theta)\begin{pmatrix} C_1 & 0 \\ 0 & C_2 \end{pmatrix}\mathbf{R}^t(\theta)\begin{bmatrix} 0 & Z_0(\omega) \\ -Z_0(\omega) & 0 \end{bmatrix}. \qquad (5)$$

Without information from shorter periods, the 2-D distortion matrix in combination with the 3-D distortion matrix (3) represents a net effect which cannot be distinguished from 3-D distortion of 1-D data. In other words, without *a priori* information the 2-D strike is not well determined. This relates very strongly to the 2-D–2-D distortion decomposition of Zhang *et al.* (1987).

The normalized error plot (Fig. 5) is a non-linear mapping of the error which varies rapidly in the best fit and worst fit regions but only gradually in between. Thus, the error information is normalized to highlight best fit (red) and worst fit (blue) and clearly indicates the correct strike. Note also the general bandedness of this figure with a kink at those periods where the fields become more sensitive to the 2-D structure. The dark blue band (worst fit to regional strike) generally follows the yellow bands (0°) for the shear and twist angles. This is, therefore, simply the 2-D model parameterization fit since model (3) reduces to model (2) when shear and twist are both zero. Of course, the worst fit is for 2-D with only five free parameters. The question of the appropriate number of free parameters will be addressed below.

Linear vertical bands of constant colour in the 3-D parameters (twist, shear and current channelling polarization azimuth) indicate frequency independence of these parameters and thus possible 3-D galvanic distortion. The current channelling azimuth can be highly constrained by the local conducting structure and may be largely independent of the regional response. If a model is chosen in which both the twist and shear are independent of frequency for the entire band, then a low γ^2 residual is obtained only for the correct 2-D strike (or the orthogonal direction).

Figure 6 presents the parameters and fit for model (3) for the same data as in Fig. 5, with no constraints. In Fig. 6[ii],

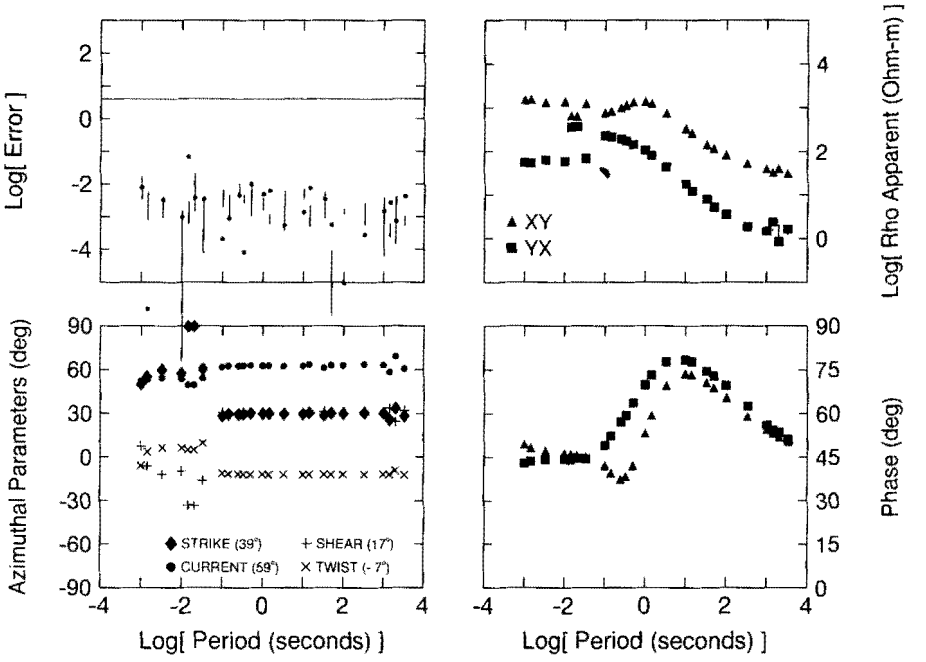

Figure 6. The residual error, strike, twist and shear, regional impedance estimates and channelling azimuth for an unconstrained 3-D model parameterization of 3-D data with 0.1 per cent noise.

for periods longer than 0.1 s, a strike direction (diamonds) is obtained which is reasonably close to the correct strike of 30°. However, at the shortest periods, the combination of a strike which is physically poorly defined, and the phase effects caused by the anomalous magnetic field of the current channelling, have disrupted the strike determination. The twist and shear parameters are almost frequency independent at periods longer than 0.1 s. However, at the shorter periods, these parameters vary with period as they are functions of the determined strike direction. The regional phases (Fig. 2a) are well recovered, as are the shapes of the regional apparent resistivities, while the local anisotropy has split the regional responses even at the highest frequencies.

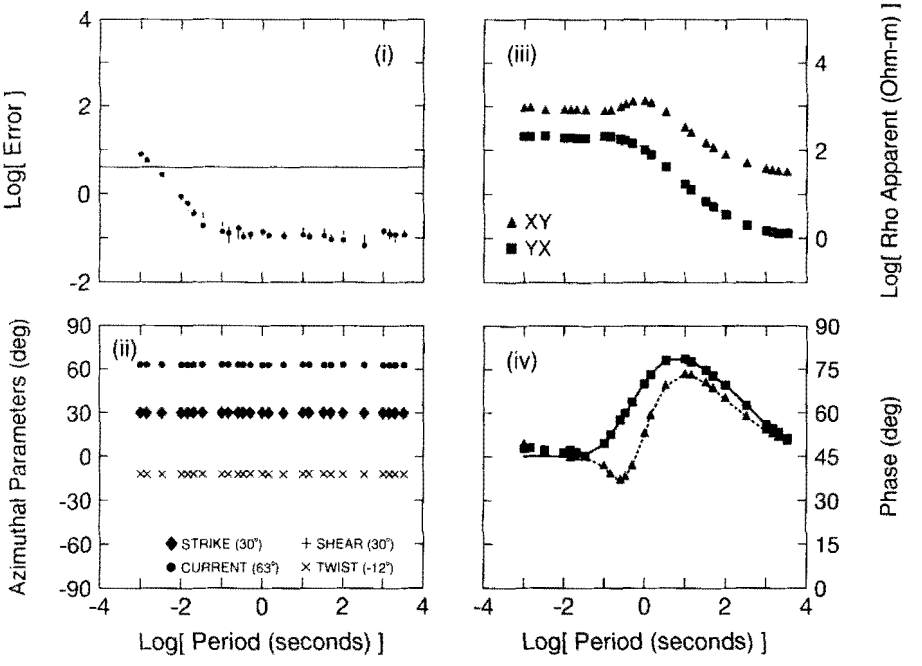

Figure 7. The residual error, strike, twist and shear, regional impedance estimates for a fully constrained 3-D model parametrization of 3-D data with 0.1 per cent noise. The solid and dashed lines show the true 2-D phase responses (Fig. 2) parallel and perpendicular to the regional strike.

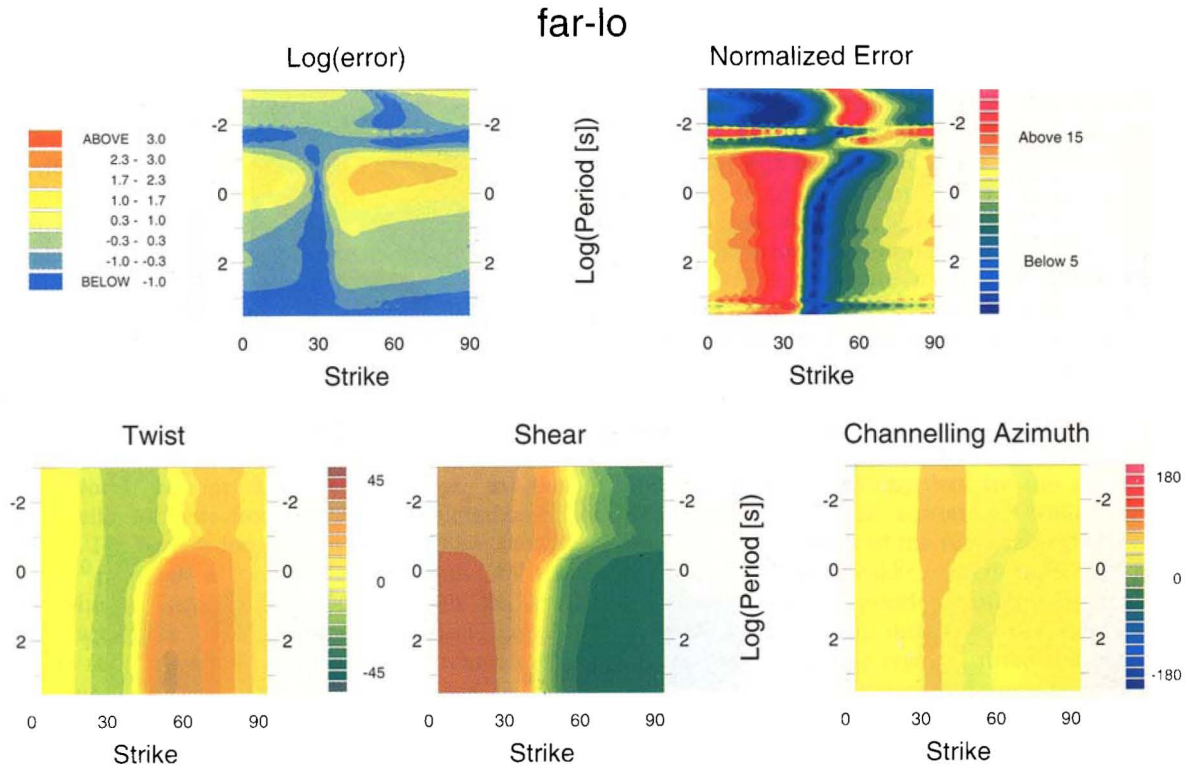

Figure 5. The logarithm of the residual error, the relative or normalized error, the twist and shear angles, and an estimate of local current polarization azimuth (channelling azimuth) for synthetic 3-D data with 0.1 per cent noise contoured as functions of strike angle and period (see text for details).

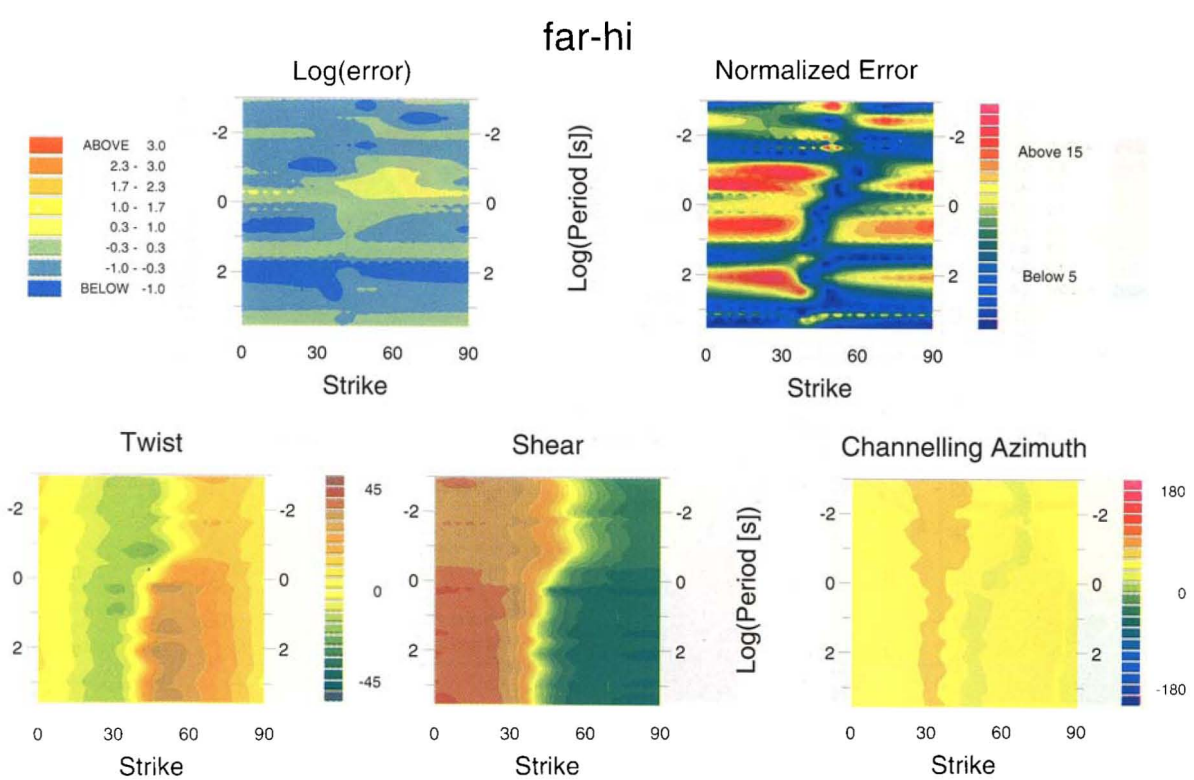

Figure 8. The chi-square residual error, normalized error, twist and shear angles and channelling azimuths for synthetic 3-D data with 2 per cent noise as functions of strike angle and period.

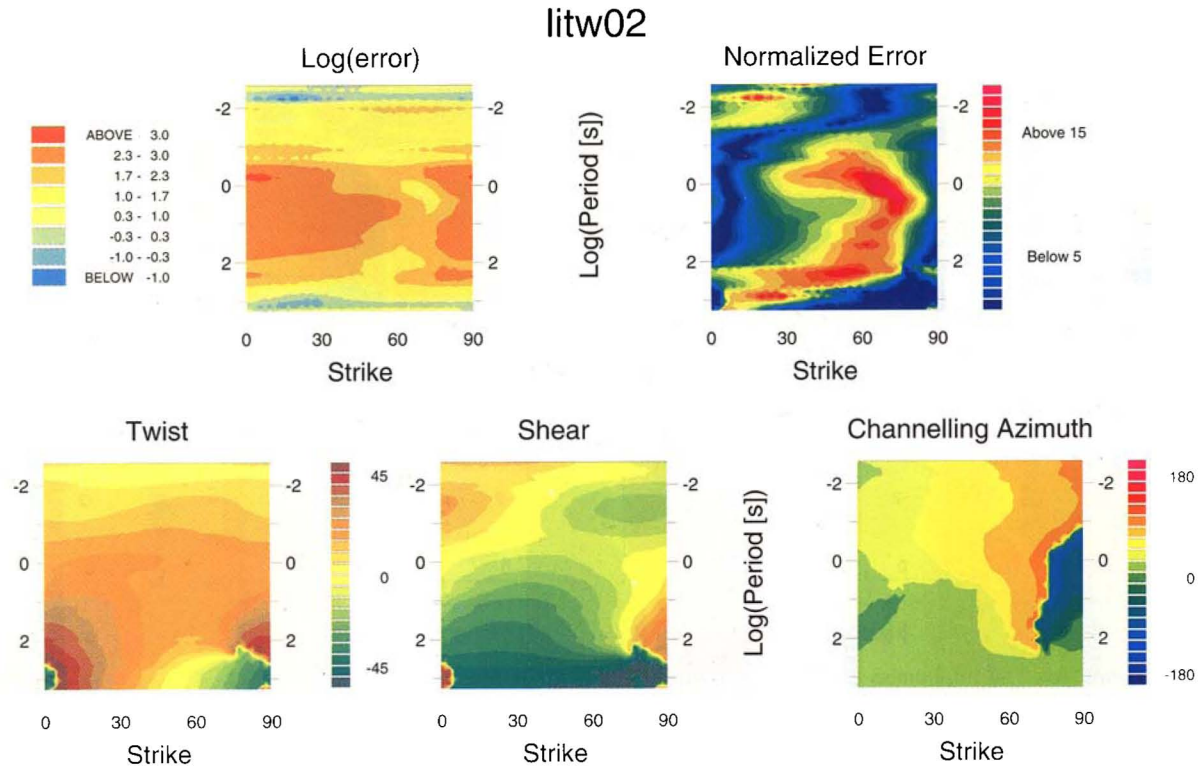

Figure 17. The chi-squared residual, normalized residual and distortion parameters for a 3-D parameterization of the data from site LITW02 as a function of regional strike and period.

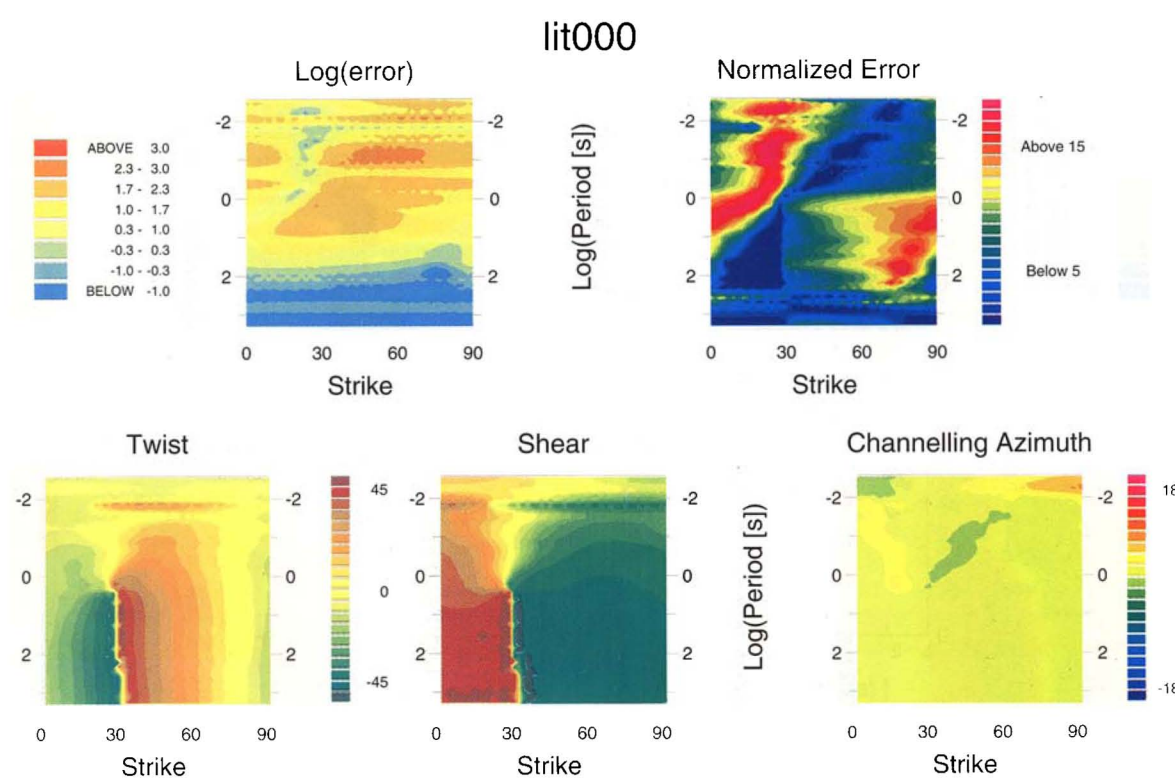

Figure 23. The chi-square residual, normalized residual and distortion parameters for a 3-D parameterization of the data from site LIT000 as a function of regional strike and period.

In this synthetic data example, a relatively *smooth* model is expected which suggests that the twist, shear and regional strike should be independent of frequency. This example illustrates the trade-off between the smoothest or simplest model (i.e. least parameters) and the lowest average residual. Although the residual plot of Fig. 6 indicates an extremely good fit to the data, the model is rather rough as the 3-D parameters and the 2-D strike are free to vary at each period. Thus, one may argue that the improved fit is due merely to the use of more parameters.

We now consider the resolution and stability of the decomposition parameters in the presence of noise. Figs 5 and 6 would indicate that a constrained strike of about 30° over the entire period range and frequency-independent 3-D parameters (twist and shear) should fit the data adequately. Fig. 7 shows such a decomposition model. Note that the estimate of local current azimuths is close to the short-period strike estimate from the 2-D parameterization model (Fig. 4). For periods longer than 0.1 s we have shown that we can produce a smooth model with $4N+3$ parameters with an acceptable residual which fits the required characteristics of the *a priori* physical model. However, for shorter periods the residual increases to a maximum value near five. This poor fit is due to the anomalous galvanic magnetic field which can be seen in the fit to the scaled data plots (not shown for this case). Some of the misfit, however, has been absorbed by alterations to the phase of the regional impedances. Note that the short-period phases are gradually rising instead of asymptotically approaching 45°. The maximum error in regional phase estimation is about 4° and decreases with increasing period due to the general $\sqrt{\omega}$ fall off of this second-order 3-D effect. The regional phases for the remainder of the periods are recovered very accurately for this low-noise level. There are also small effects on the shape of the apparent resistivity curves due to this anomalous magnetic field. The remaining effects on the apparent resistivity (Fig. 7[iii]) due to the local anisotropy and gain will be discussed below.

The stability of parameters in the presence of noise is an important facet of this study. Fig. 8 utilizes the same data as Fig. 5, but with noise added at the 2 per cent level, which is more typical of experimental data. Notice that the correct strike is less resolved by both the γ^2 residual and the normalized error. Only in the narrow period band from 0.1 to 10 s where there are strong differences between the phases of the regional TE and TM modes (Fig. 2a) is the strike determined. However, the twist and shear angles and channelling azimuth have varied only slightly from Fig. 5. Several synthetic studies have shown that the distortion parameters are significantly more stable in the presence of noise than is the 2-D strike (Jones & Groom 1993). This is understandable considering that, for this example, the 3-D effects are first-order scattering, while the inductive response (contribution of the vector potential) from the 2-D structure is a much weaker scattering effect. Generally, the 2-D strike is a very poorly constrained parameter in the presence of 3-D static distortion and noise. This is why methods for recovering regional strike and phase responses based solely upon rotating the impedance tensor (Bahr 1988, 1991; Chakridi *et al.* 1992) are unstable for galvanically distorted data (Jones & Groom 1993).

Examining Fig. 8 suggests that constraining the twist and shear to be independent of frequency will result in a low γ^2 at *all* periods only for regional strike angles which are approximately correct (i.e. 25°–35°). Constraining the strike (figure not shown) to lie between 25°–35° produces relatively frequency-independent shear, twist and current azimuth. When the strike, twist and shear are constrained to be the mean parameters of this model, the parameterization of Fig. 9 is obtained. The azimuthal parameters (Fig. 9[ii]) are slightly different from those for the low-noise data (Fig. 7).

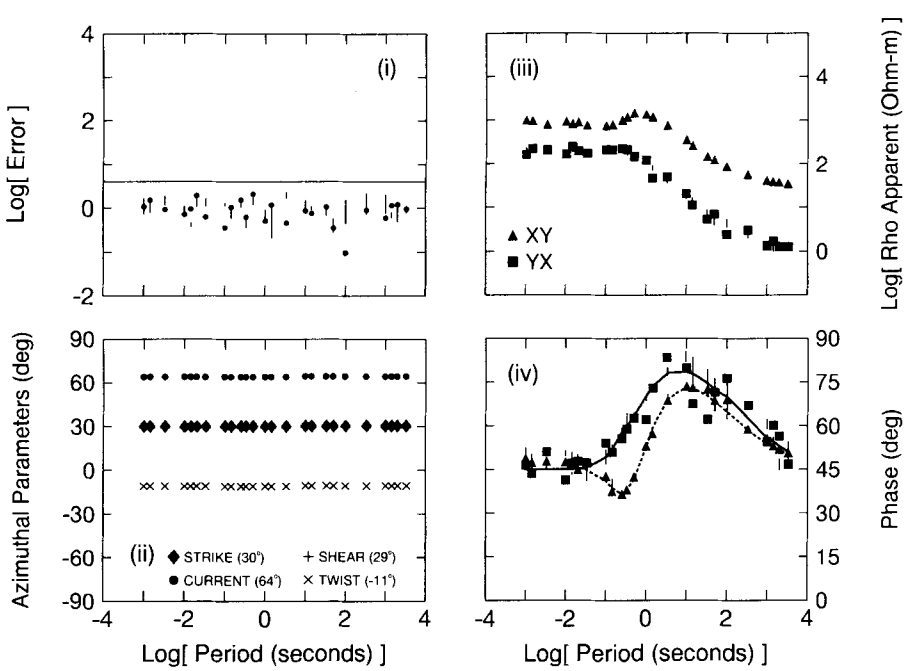

Figure 9. The residual error, strike, twist and shear, and regional impedance estimates for a constrained 3-D model parameterization of 3-D data with (2 per cent) noise. True regional phase responses are given for comparison.

The regional impedance (Fig. 9[iii]) estimates are close to the low-noise estimates, although the phases (Fig. 9[iv]) deviate somewhat more from the true phases and are more erratic. The misfit residual is about 1 at all periods and this smooth model fits the data well (again not shown). The regional phase estimates are still disturbed at high frequencies (Fig. 9[iv]) by the magnetic field, due to the 3-D structure, but now any inadequacy in the underlying model cannot be determined with this noise level (Fig. 9[i]).

Improved estimates of regional apparent resistivities

In some cases, it is possible to correct for the effects of local distortion on the amplitudes of the regional apparent resistivity estimates. The decomposition method used here assumes that the interpreter cannot distinguish between regional and local anisotropy. That is, any regional and local anisotropy which are developed along the same coordinate axes cannot be distinguished *a priori* (GB1). Thus, the regional impedance estimates from model (3) are actually

$$g(1+s)Z_{\perp} \quad \text{and} \quad g(1-s)Z_{\parallel} \tag{6}$$

where the anisotropy parameter, s, lies within $(-1, 1)$. If, however, one can determine the regional anisotropy then the local anisotropy can be corrected by simple algebraic methods.

In our experimental experience, often the anisotropy at the high end of the frequency range is due to structures which are small compared to the survey scale and the site density. In these cases, this anisotropy can be adjudged local or uninterpretable due to inadequate field sampling. The synthetic example is a case in point. An examination of Figs 5 and 8, along with impedance phase information, indicates that there is little or no preference for 2-D strike until periods are longer than 0.1 s. For the short periods, all the anisotropy is local and related to the other 3-D effects seen in Figs 7 and 9. Therefore, at short periods, what is recovered by the decomposition is often approximately

$$g(1+s)Z_0 \quad \text{and} \quad g(1-s)Z_0 \tag{7}$$

where Z_0 is the underlying regional response which is 1-D. The value of the anisotropy parameter, s, can now be estimated by some simple algebra. The method chosen here is to average the estimates of s at each period over some preferred period range determined from decomposition analyses of the data. Once s is estimated, it can then be removed from both impedance estimates (6) throughout the entire period range. This is valid since, as a galvanic scattering effect, it persists for all longer periods. Fig. 10 shows the resulting corrected regional apparent resistivities for low- and high-noise levels compared to the actual regional estimates. For this synthetic data, the actual electric distortion matrix **C** is known analytically and there exists an analytic decomposition of **C** into its constituent parts (GB1). Thus, the impedance decomposition and anisotropy correction can be verified. Clearly the recovered shapes are correct while much of the 3-D effects on the magnitudes of the ρ_a have been removed. Comparing Figs 3(a), 7 and 10 shows that the primary effects of the electric distortion are due to the effects of shear, twist and anisotropy rather than an intrinsic level change. These three effects cause both

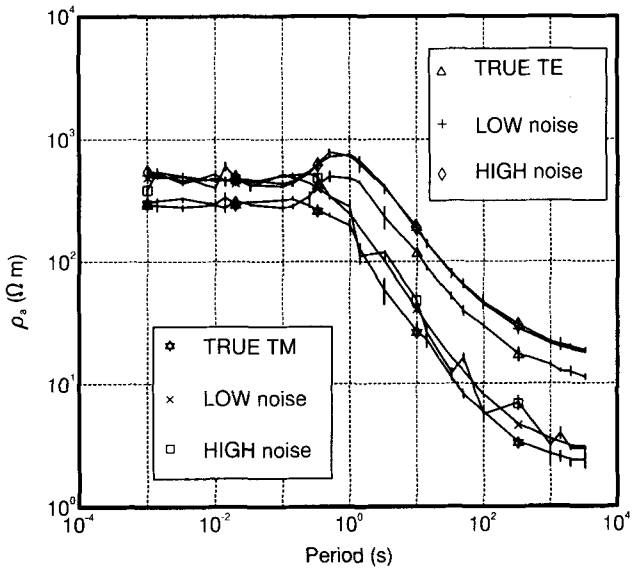

Figure 10. Comparison of estimated regional apparent resistivities after anisotropy correction. Low noise 0.1 per cent. High noise 2 per cent.

the mixing of the regional responses into the four elements of the impedance tensor thus distorting the phase information as well as causing much of the magnitude distortions. The result is independent of whether the hemisphere is resistive or conductive but is true only for sites outside the anomaly. If the site were inside the out-cropping hemisphere, the impedance tensor would appear 2-D (i.e. no shear, twist or anisotropy) due to the symmetry of the hemisphere, but the gain factor would be important. The apparent resistivity levels would be depressed significantly for a conducting hemisphere or enhanced for a resistive hemisphere. However, if the heterogeneity did not outcrop, then the magnitude shift of the scaling parameter (g) would be reduced even for sites over the anomaly (Pellerin & Holmann 1990). Building distortion matrices, **C**, via a variety of numerical methods and then decomposing the distortion matrices (GB1) into their constituent parameters (i.e. g, s, t, e) verified these conclusions.

Final gain level correction

The apparent resistivities determined from model (3) are scaled relative to the true 2-D responses by a multiplicative factor of about 1.6 (the impedances by 1.25). The final site-gain scaling effect should normally be addressed by other techniques for it cannot easily be determined from analysis of the tensor data alone. The difficulty is that there are two level changes; one associated with the 3-D structure and one with the 2-D structure.

To appreciate the two level changes, we examine the 1-D inverse model derived from two standard 1-D estimators. The first estimator is simply the square root of the determinant of the impedance tensor (DA) while the second is the arithmetic average (TA) of the off-diagonal elements (Berdichevsky & Dmitriev 1976). Impedance level problems expected for both the estimators, DA and TA, are associated with two galvanic effects, one 2-D and one 3-D.

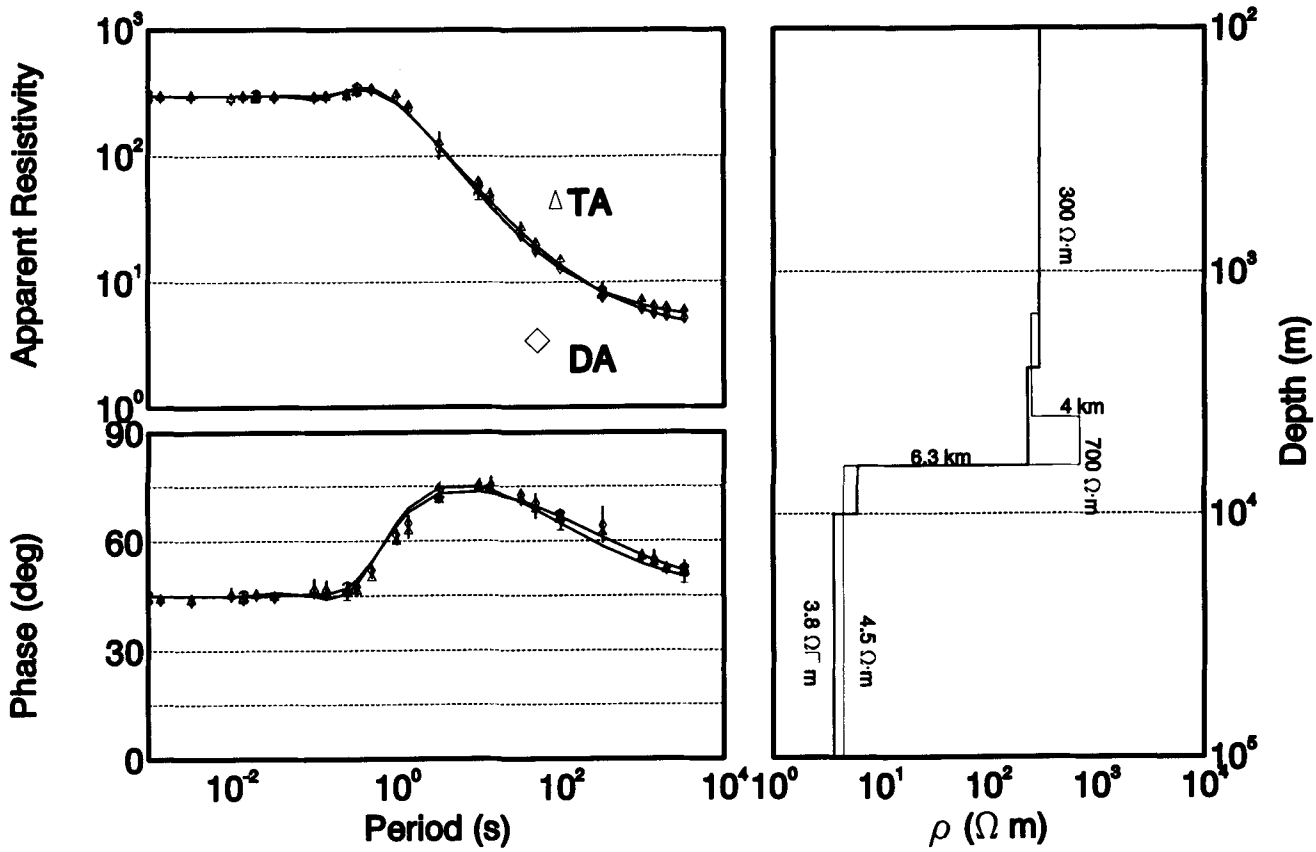

Figure 11. 1-D resistivity and phase responses (left panels) for the minimum structure inverse model from DA (bold line) and TA estimates for the true regional response plus noise.

Figure 11 contains the DA and TA estimators and their minimum-structure inverses (Constable, Parker & Constable 1987) for the true regional data at the site with the 3-D anomaly removed and for a moderate noise level. An iterative method of inversion sought a small misfit with minimum structure beginning with a half-space model having the true resistivity of the upper layer. The long-period apparent resistivity of the DA is slightly lower than the TA, but the two are roughly parallel. Apart from the fact that the DA is here not sensitive to the resistive layer (3000 Ωm, Fig. 1), the models are very similar, both underestimating the depth to the second contact, and recovering a substratum resistivity less than half the true value. This can be understood by considering that at the long periods the 2-D structure has only a galvanic effect with no phase difference between TE and TM. In the regional strike system with sufficiently small ω, from (5) one obtains

$$\bar{\bar{Z}}_{2\text{-D}}(\omega) \approx g_{2\text{-D}} \begin{pmatrix} 1+s_{2\text{-D}} & 0 \\ 0 & 1-s_{2\text{-D}} \end{pmatrix} \times \begin{bmatrix} 0 & Z_0(\omega) \\ -Z_0(\omega) & 0 \end{bmatrix}, \quad |s_{2\text{-D}}| < 1. \tag{8}$$

Thus there is a site gain ($g_{2\text{-D}}$) and an anisotropy ($s_{2\text{-D}}$) associated with the 2-D response (GB2). ($s_{2\text{-D}}$) represents the amount of apparent resistivity splitting in the 2-D impedances and ranges from $(-1, 1)$. The TA response recovers, in the terms of these parameters, $g_{2\text{-D}}Z_0$ while the DA recovers $g_{2\text{-D}}Z_0(1-s_{2\text{-D}}^2)^{1/2}$. Thus unless $|s_{2\text{-D}}|$ is near one, the two estimates will be close.

Figures 12(a) and (b) show the DA and TA estimators and their four layer inverses for the 2 per cent noise level 3-D synthetic data. Comparison of the DA estimator with the TA shows the better statistical stability of the TA as an estimator especially for the phases as indicated by the variance bars on the estimators. At this site (chosen to have only moderate current channelling effects), the TA overestimates the top layer resistivity, is not strongly sensitive to the resistive layer, and underestimates the depths to both contacts. However, the TA estimates the basement resistivity better than the DA. The determinant of the electric distortion matrix is close to 1 at 0.96. Thus the determinant average apparent resistivity is reduced only by approximately 0.92 from the determinant average of the regional response. As a result, the DA estimates the upper layer quite well at 275 Ωm. The resistive layer is not detected while the depth to the second contact is underestimated and the basement resistivity is three times too small. These results should not be construed as general implications, but are rather due to the specifics of the responses both 2-D and 3-D. In particular, there are other cases where the DA is an extremely poor estimator. Whenever the current channelling is severe, the electric currents are constrained to flow locally in one direction independent of the direction of the horizontal magnetic field vector. In this case, since the impedance tensor is a linear

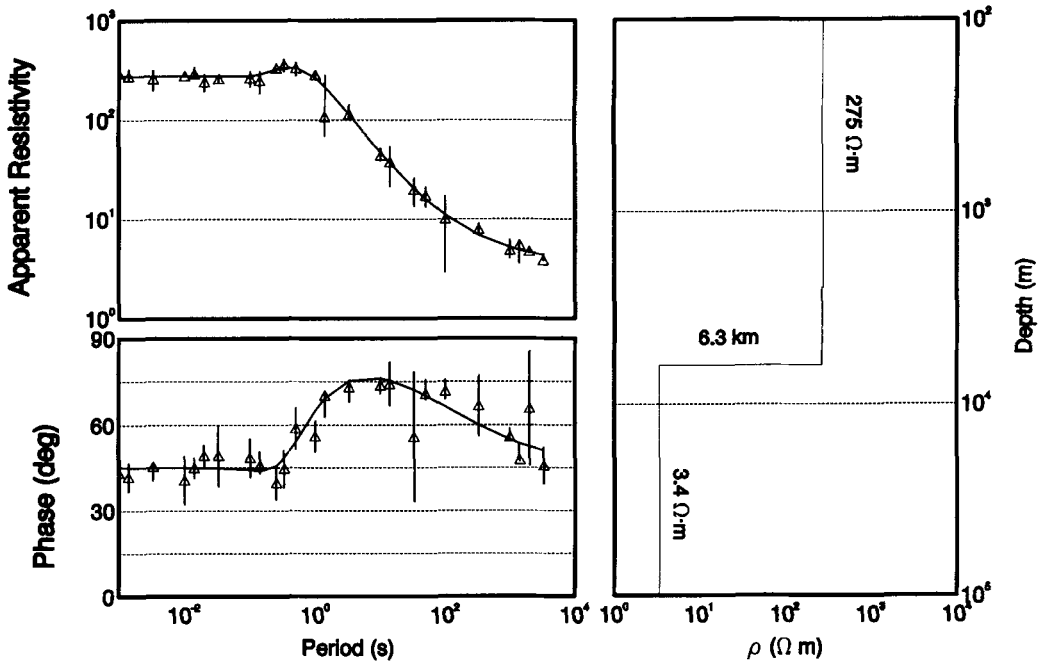

Figure 12(a). Minimum structure 1-D inverse of determinant average (DA) of 3-D synthetic data with (2 per cent) noise.

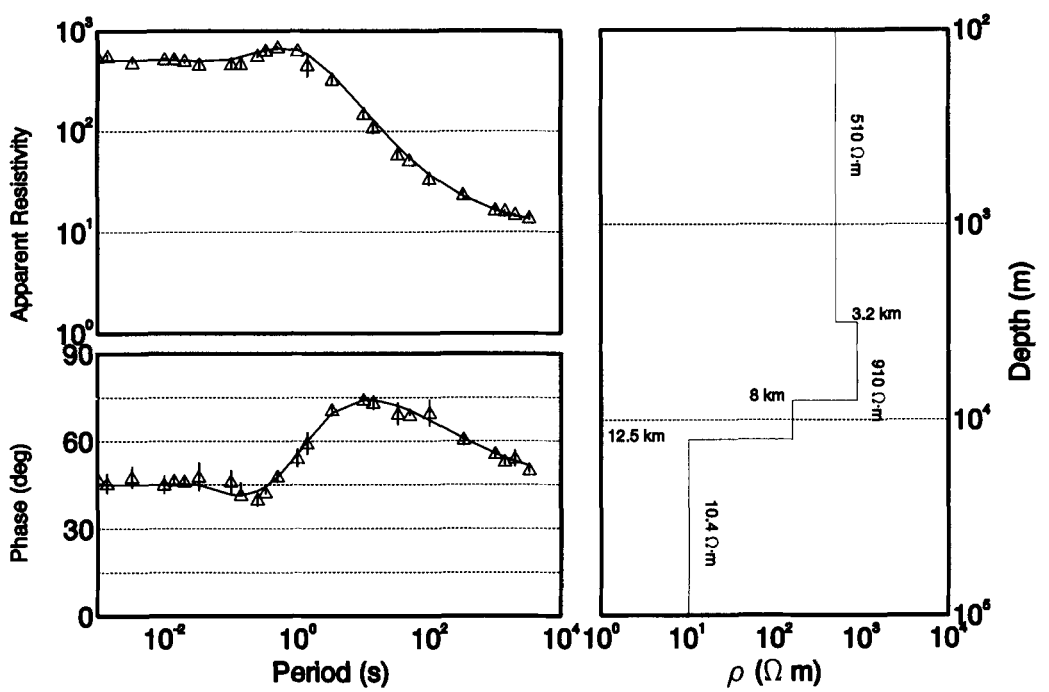

Figure 12(b). Inverse of anti-trace average (TA) for same data.

transformation between magnetic and electric field vectors, the tensor will be almost singular as it maps a 2-D magnetic vector space to a 1-D electric vector space. In this case, the phase of the DA is almost indeterminate which adds to the already unstable phase estimates generated by a multiplicative average.

Comparing Figs 11 and 12(a, b), note that for the DA, the 3-D effect has only slighly modified the 2-D response while increasing the resistivities for the TA model. However, much of the long-period level problem and resulting inversion value for the substratum resistivity is associated with the 2-D site-gain level, not that of the 3-D structure. That the inverted substratum for the TA of the 3-D data is close to the correct regional substratum resistivity is merely fortuitous.

The decomposition trace 1-D estimator

It is difficult to rationalize theoretically the use of either of the aforementioned 1-D estimators for a general 3-D

scattering problem. There are, however, theoretical arguments for the anti-trace, or Berdichevsky average, in a 2-D environment. In addition, the arithmetic average is clearly more stable in the presence of noise with strong galvanic effects. We derive another arithmetic 1-D estimator that extends the rational used for the TA in a 2-D environment to 3-D environments. It can be understood by realizing that the decomposition of Groom & Bailey (1989) actually recovers estimates of a 2-D impedance that is an extension of (8), namely

$$\bar{\bar{Z}}_{2\text{-D}}(\omega) \approx g_{3\text{-D}}\begin{pmatrix} 1+s_{3\text{-D}} & 0 \\ 0 & 1-s_{3\text{-D}} \end{pmatrix} g_{2\text{-D}}\begin{pmatrix} 1+s_{2\text{-D}} & 0 \\ 0 & 1-s_{2\text{-D}} \end{pmatrix} \times \begin{bmatrix} 0 & Z_0(\omega) \\ -Z_0(\omega) & 0 \end{bmatrix}, \quad |s_{i\text{-D}}| < 1. \tag{9}$$

In (9) the first two operators are the 3-D site-gain and anisotropic effects, whereas the next two are those of the 2-D structure as in (8). Thus, there are two level effects and two anisotropy effects. Taking the anti-trace average of this tensor, which is equivalent to averaging the estimates of impedance from the decomposition (GB1), results in a 1-D estimator called herein the decomposition anti-trace average, (DTA), which is $g_{2\text{-D}}g_{3\text{-D}}[1+(s_{2\text{-D}}s_{3\text{-D}})]Z_0$. Now we see clearly the two level problems in the 3-D–2-D data. If, for example, the regional structure was 1-D, then this estimator recovers simply $g_{3\text{-D}}Z_0$. We have seen (Fig. 10) that the site-level effect $g_{3\text{-D}}$ is a small 3-D effect compared to others (which we have removed) unless the site is inside the 3-D scatterer. If the structure is truly 2-D, or the tensor appears 2-D due to the symmetry of the 3-D body, then TA and DTA are equivalent.

Figure 13 presents the minimum-structure inverse of the DTA for the 3-D data used for Fig. 12 with high noise. A minimum of five layers were required to fit the DTA estimator at the misfit levels of Figs 11 and 12(a, b). The DTA (Fig. 13) produces a slightly better estimate of the upper level resistivity than TA. Once the magnetic 3-D effects have decayed, the upper level resistivity is reasonably well estimated (i.e. 350 Ωm) as galvanic effects in the magnetic fields bias the resistivity and thickness of the first layer. The DTA is sensitive to the second resistive layer while the depth to basement and the basement resistivity are well estimated.

The preferred estimator is, in our opinion, dependent upon the conductivity distribution. Arguments may be found for each depending on the specific structure, site location and noise levels. Generally, the DA can be extremely unstable when there are large galvanic effects (2-D or 3-D) polarizing the electric field. The DTA and TA generally are similar in magnitude but the DTA, because it derives from a method which is designed to recover the shapes of the regional responses, is more likely to maintain the small changes in these shapes due to moderately thick resistive layers. For the hemisphere scatterer, from a study of many sites in and around the structure, the DTA is preferred particularly if the background structure is 1-D. These estimates, after decomposition and anisotropy correction, still contain a remnant static shift factor, albeit rather small. Most importantly, for the techniques described herein, using the DTA in conjunction with the use of other EM methods may allow the recovery of the correct level for the regional apparent resistivity estimates (e.g. Fig. 10).

Another 1-D estimator of interest, particularly where the site is on the conductive side of a 2-D contact, is the TE response. Prior to decomposition, inversion of a single impedance element (possibly after rotation) can lead to erroneous interpretations if the 3-D scattering is significant. This can occur even when the correct regional TE mode direction is known from other sources. After 3-D

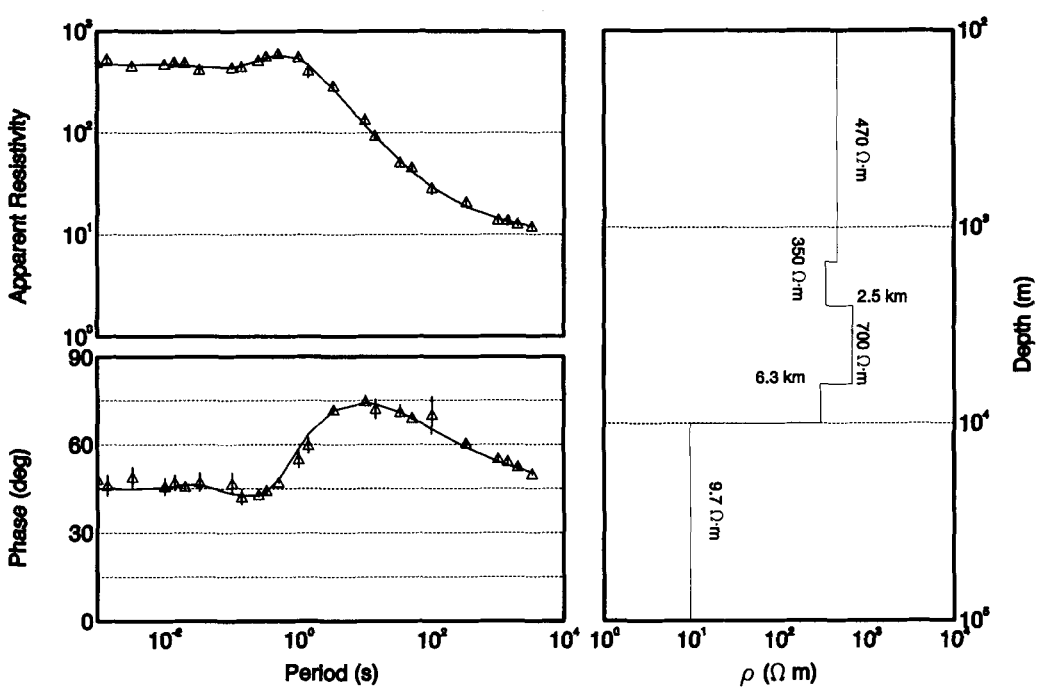

Figure 13. Decomposition Trace (DTA) for synthetic 3-D data and 1-D model responses (left panel) for the resistivity model (right panel) determined by a minimum structure inversion.

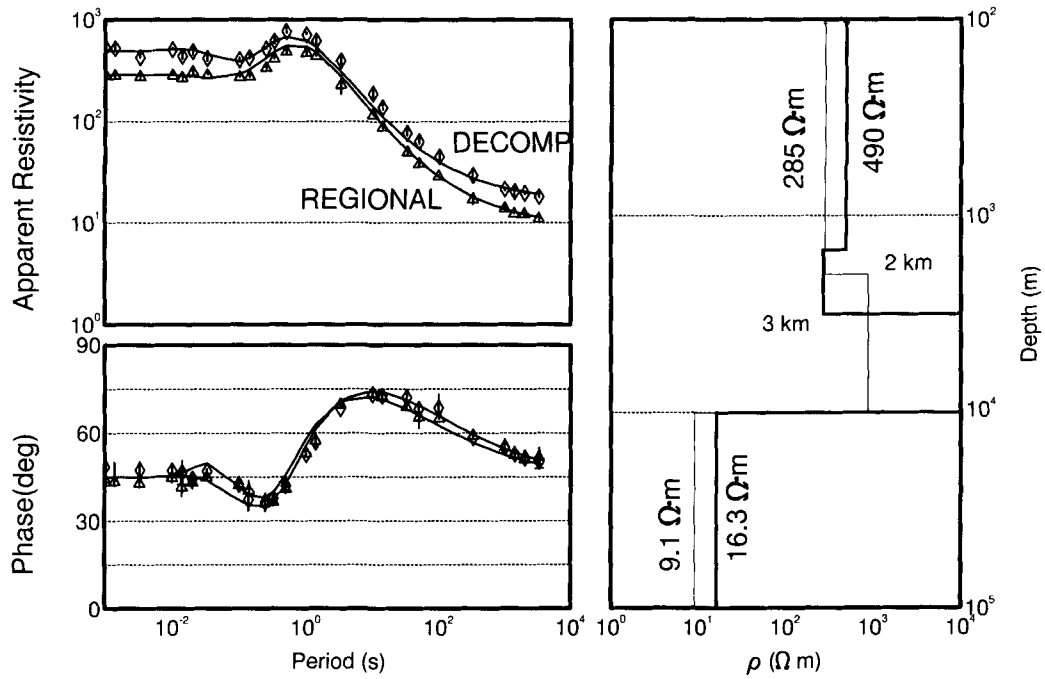

Figure 14. Comparison of the true regional TE 1-D inverse to estimated regional TE inverse after all 3-D corrections. In the right panel, the bold line represents the model from the 3-D data after decomposition.

decomposition has recovered the correct phases and removed all but the site gain (Fig. 10), one could model one-dimensionally the TE mode without any further correction when the TE–TM ambiguity has been resolved. Fig. 14 presents a minimum-layer 1-D inversion for the TE mode response for both the true 2-D impedances and the estimated 2-D impedances from the 3-D data after all 3-D corrections (i.e. decomposition plus local anisotropy removal). Comparison of estimated and actual impedances (Fig. 14) indicates what remains of the 3-D scattering. The phases are essentially equivalent within the noise except for some high-frequency distortion due to the 3-D magnetic effects, and the apparent resistivities are parallel, but the 3-D level is now shifted upwards only slightly from the true response. The true 2-D response recovers the basement resistivity and the basement contact accurately, and is sensitive to the resistive layer. However, the 2-D induction modifies the depth to the first contact as determined by the 1-D inversion. The improved estimate of the first contact depth is fortuitous and not generally significant. A surface resistive layer is recovered from the estimated impedance to fit the 3-D magnetic effects. No intermediate layer is required (Fig. 14) between the resistive layer and the basement to fit the data, and the depth to basement is determined accurately. Outside a resistive 3-D anomaly, the contact depths would be made shallower. This inversion of the 3-D data is certainly more accurate than any of the others (TA, DA, DTA or either impedance from a 2-D decomposition).

AN EXAMPLE WITH FIELD DATA

With actual field data the application of the decomposition or parameterization analysis process can be more difficult because of poor data and uncertainty in the variance estimates. Also, 3-D induction may be important and the physical parameterization may not be correct for such scattering. To indicate both the usefulness and the difficulties in applying this methodology, data from two closely spaced sites from an MT survey conducted in the Canadian Southern Cordillera (Jones *et al.* 1988) are analysed. The general trend of the exposed geological structures throughout the region is N30°W, although one site (LIT000) lies in a valley following the Eocene extensional Slocan Lake Fault, which locally strikes about N30°E. The fault dips east beneath the Nelson Batholith and has been imaged seismically to depths of 25 to 30 km (Cook *et al.* 1988). The valley contains relatively conducting sediments. The other site (LITW02) is located 15 km to the west within the Valhalla Gneiss complex on the flanks of a glacial valley.

Figure 15(a) presents model 2 (i.e. 2-D) parameters and residual errors for the western site, LITW02. Both the residual error and skew plots show similarities to the synthetic 3-D example discussed in the previous section. The skew increases gradually from approximately zero to a long-period asymptote. This response could be due either to 3-D effects becoming dominant at longer periods, or to the advent of 2-D effects coupled with a local, short-period, 3-D response. The residual errors are probably acceptable to periods of about 0.1 s, but then increase to values greater than 1000. There is a decrease in the misfit at long periods, but this is probably the result of an increse in the variance estimates. The minor impedance phase increases to values greater than 90°, a fairly common occurrence for a 2-D parameterization (Groom & Bahr 1992), and occurs at many of the sites in this survey. Again, the comparison plots of the data and the model parameterization results (Fig. 15b) indicate that the off-diagonal elements of the tensor are well

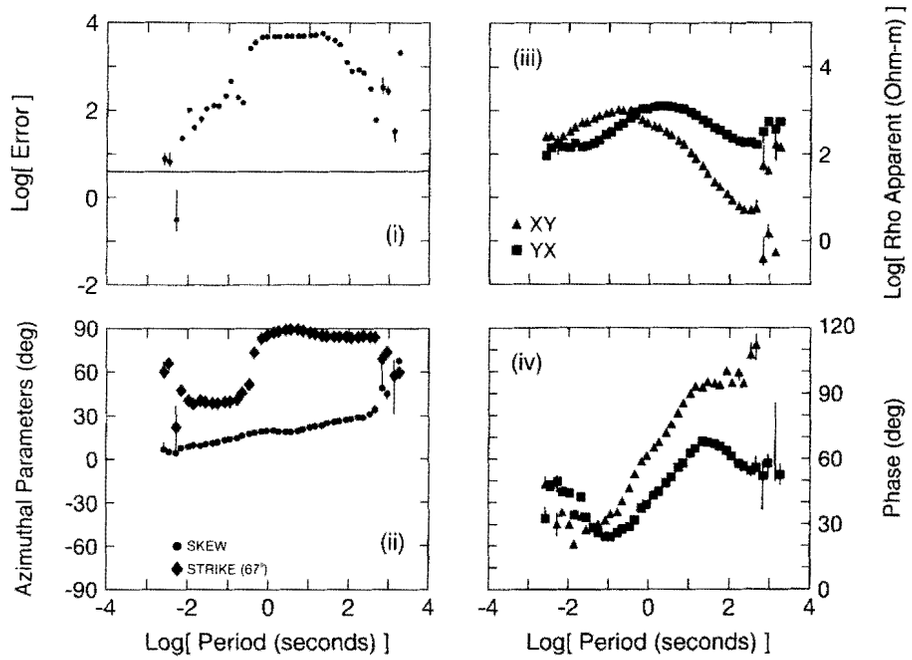

Figure 15(a). The 2-D model parameters for field data from station LITW02 for best fitting strike.

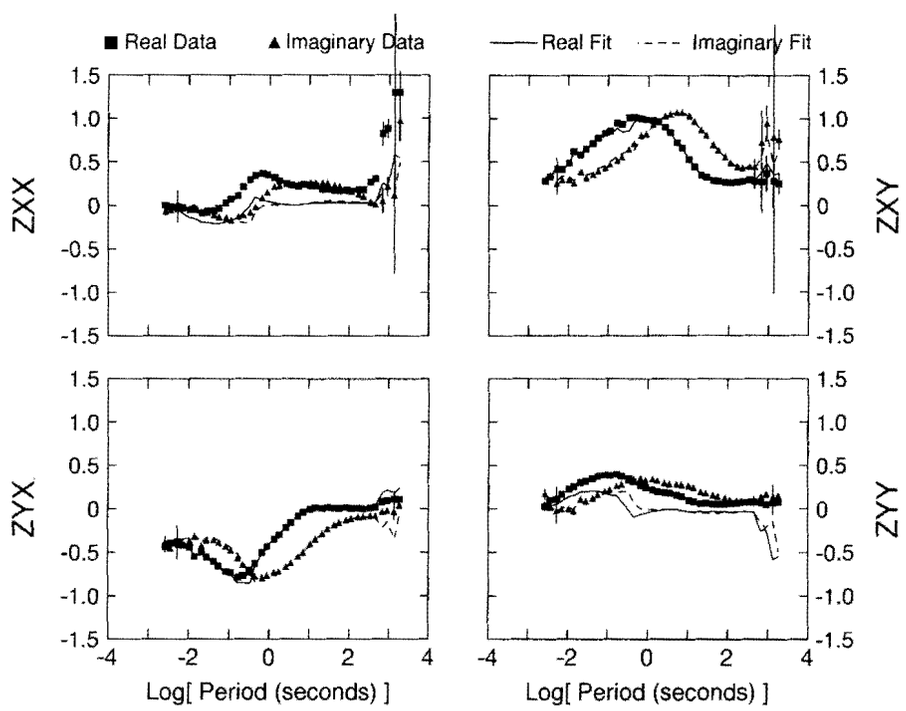

Figure 15(b). Fit to scaled impedance data.

modelled, whereas the diagonal elements are not, particularly at the longer periods. The parameterization suggests that the regional strike is approximately 90° (or 0°) but clearly, model (2) is not appropriate for these data.

Figures 16(a) and (b) show the results of applying model (3), without constraints, to these data (site LITW02). The regional strike is poorly defined for periods shorter than 0.1 s, but is fairly stable and smooth with values between 50° and 70° at longer periods. Recall that the 2-D strike and the skew also underwent a transition at 0.1 s. The short-period twist and shear are erratic, but at periods greater than 0.1 s the twist is nearly frequency independent, and the shear varies in a similar fashion to that of the strike azimuth. Since these distortion parameters are functions of the coordinate system, and the decomposition technique uses the regional strike as the definition of the coordinate system, it is

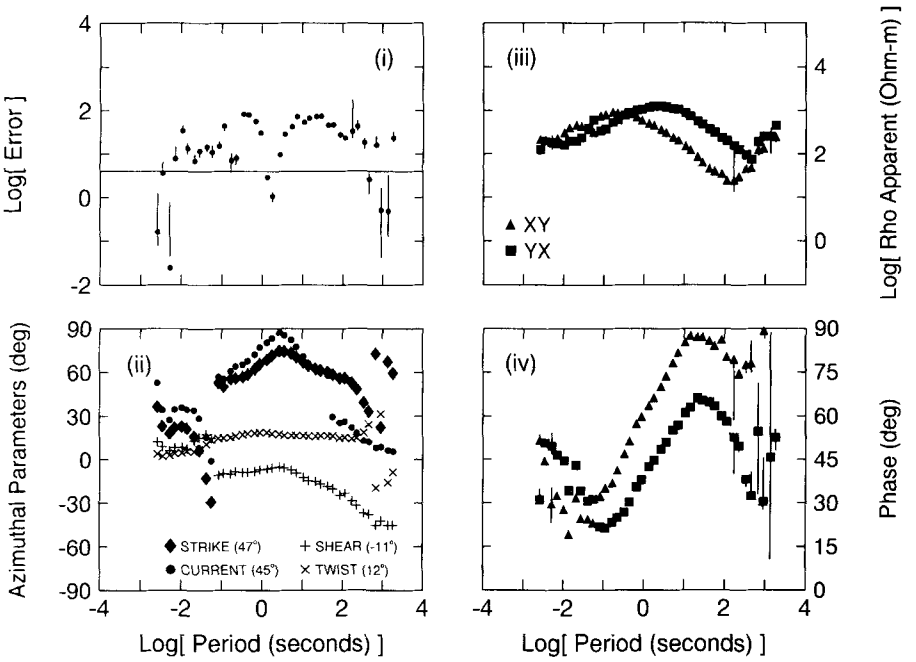

Figure 16(a). The unconstrained 3-D model parameters for field data from station LITW02.

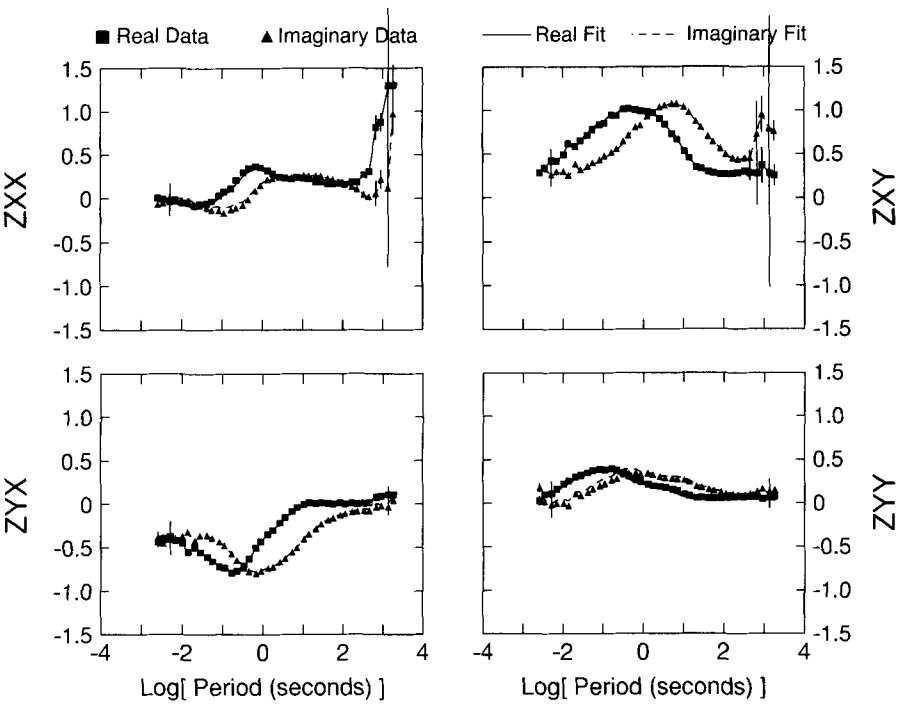

Figure 16(b). Fit to scaled impedance data.

expected that they should vary with the regional strike parameter (e.g. Fig. 5). The minor phase, although still near 90° at longer periods, remains now within the first quadrant. The residual errors have decreased by at least one order of magnitude for all periods. Fig 16(b) indicates that to a great extent this unconstrained parameterization fits the data. We now examine the significance of the variations in the azimuthal parameters.

Figure 17 indicates that while the short-period strike is poorly constrained (error and normalized error plots), there is a well-resolved long-period strike. If we seek a strike angle that has a low associated residual error, and for which twist and shear are as period independent as possible, then a fairly narrow band of rotation angle around an azimuth of

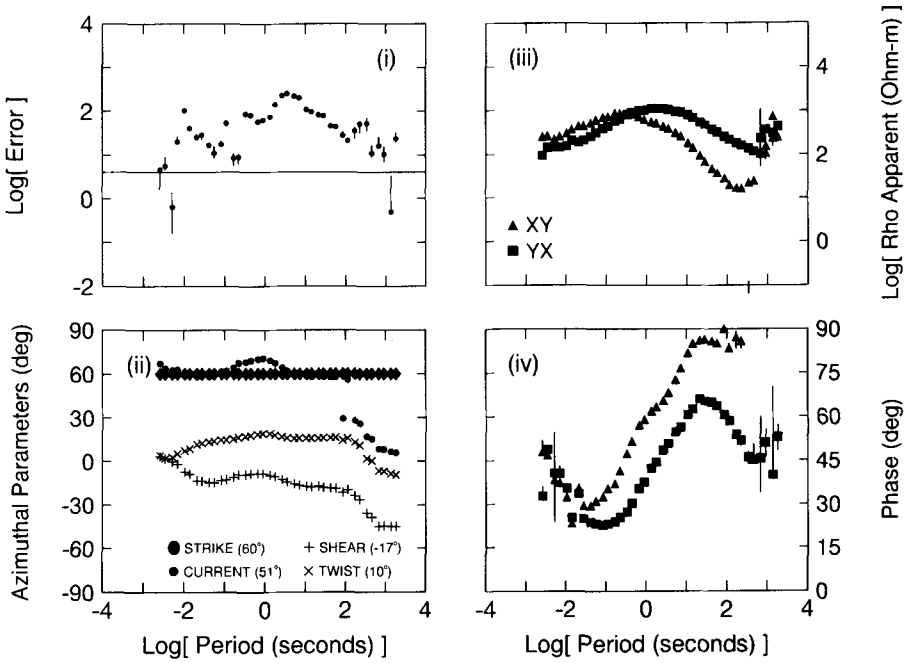

Figure 18. The 3-D model parameters for field data from site LITW02 with strike constrained to 60°.

60° is defined. Fig. 18 shows that, with the strike constrained to 60°, the twist and shear are relatively constant for periods greater than 0.03 s, while the residual error is only slightly increased over the unconstrained model (Fig. 16a). The large residual errors at frequencies between 1 to 10 Hz may be associated with poor impedance estimates or unrealistically small variances.

In Fig. 19(a), a model has been used which constrains the regional strike, twist and shear to 60°, −22° and −12° respectively, over the entire period range to fit preferentially the data at periods greater than 0.01 s. The residual error is slightly larger than for the previous model, especially for the shortest periods, but there is very little difference in the regional impedance estimates (Fig. 19b). There is a misfit near 1 s for all elements except for the Z_{xy} component. The short-period misfit in Z_{yy} is the result of constraining the azumiths preferentially for the longer periods. The long-period misfit for the real part of Z_{yy}, also apparent in the unconstrained fits (not shown), may be the result of noise bias in the data, inadequacy of the model or source field effects. It is important to note, however, that this rather smooth 3-D model fits the data well, certainly much better than the best fitting 2-D model. An additional correction was made to the regional estimates since there appears to be no strong preference for strike at short periods. A short-period anisotropy (estimated to be $s \approx 0.14$) was assumed to be entirely local and thus removed. The only remaining uncertainty is the absolute level (i.e. site gain) of the apparent resistivity curves. This problem will be addressed later.

The stable strike azimuth is determined by the high-quality data and by the strong 2-D inductive-phase response characterized by the phase split occurring over more than four decades of period. The low shear values (less than 25°, Fig. 19(a)[ii]), the weak local anisotropy (Fig. 18[iii]) and the azimuthal dependence of the channelling azimuth (lower right panel, Fig. 17) all indicate a moderate 3-D current channelling response. The persistent phase split indicates that the 2-D structure must continue to considerable depth or that there must be additional lateral 2-D contacts at increasingly greater distances and/or depths. However, this is not supported by 2-D modelling studies of MT and geomagnetic depth-sounding data collected along east–west profiles across southern British Columbia (Jones *et al.* 1988; Jones, Groom & Kurtz 1993). Another possibility is electrical anisotropy in the lower crust and/or upper mantle.

Regional large-scale geological trends are approximately N30°W in southern British Columbia. Since structural strike azimuths as determined from magnetotellurics are ambiguous by 90°, the strike direction determined from the decomposition is consistent with the geological trends. For this reason, Z_{xy} (Figs 18 and 19(a)[iii]) is considered to be the regional estimate of the TM impedance (electric fields measured perpendicular to strike). The direction of present-day large-scale tectonic stress is approximately orthogonal to the geological trends (Adams 1989).

Before continuing with the interpretation of the data from site LITW02, it is useful to examine the parameters of an adjacent site to confirm and refine our analysis. Fig. 20 shows the model (2) decomposition parameters for site LIT000. The large skew values along with one of the phase estimates increasing to values greater than 90° for periods longer than 1.0 s are indicative of strong 3-D effects. The residual error is also large for the longer periods. The response can be divided into two bands, one above 1.0 s and one below. The short-period strike azimuth is approximately N30°E, parallel to the valley (Slocan Lake) and the decomposition indicates a satisfactory fit to the data (not shown). At longer periods, the skew increases, the strike

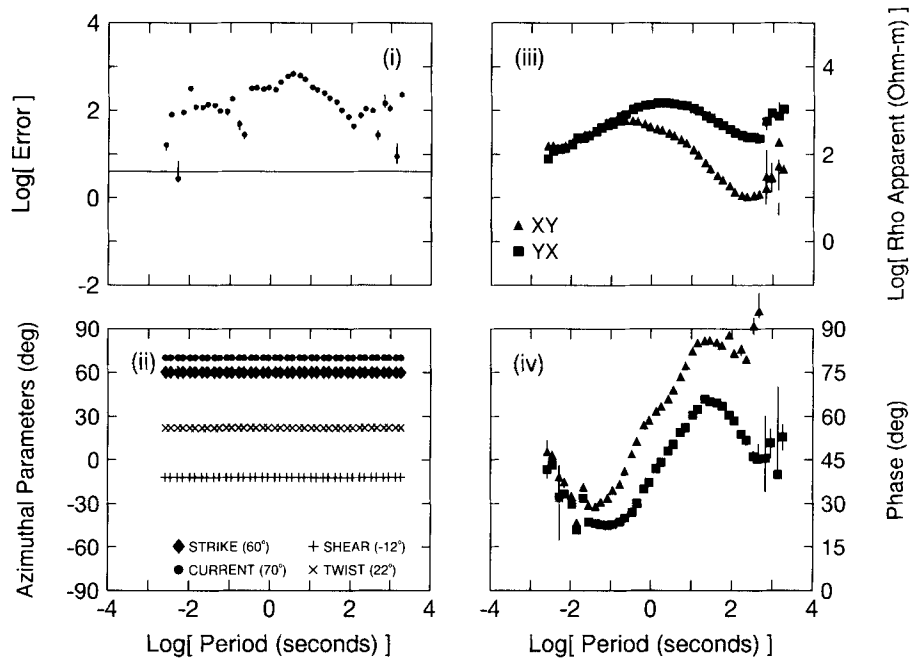

Figure 19(a). The 3-D model parameters for field data from site LITW02 for a fully constrained model after correction for anisotropy in apparent resistivities.

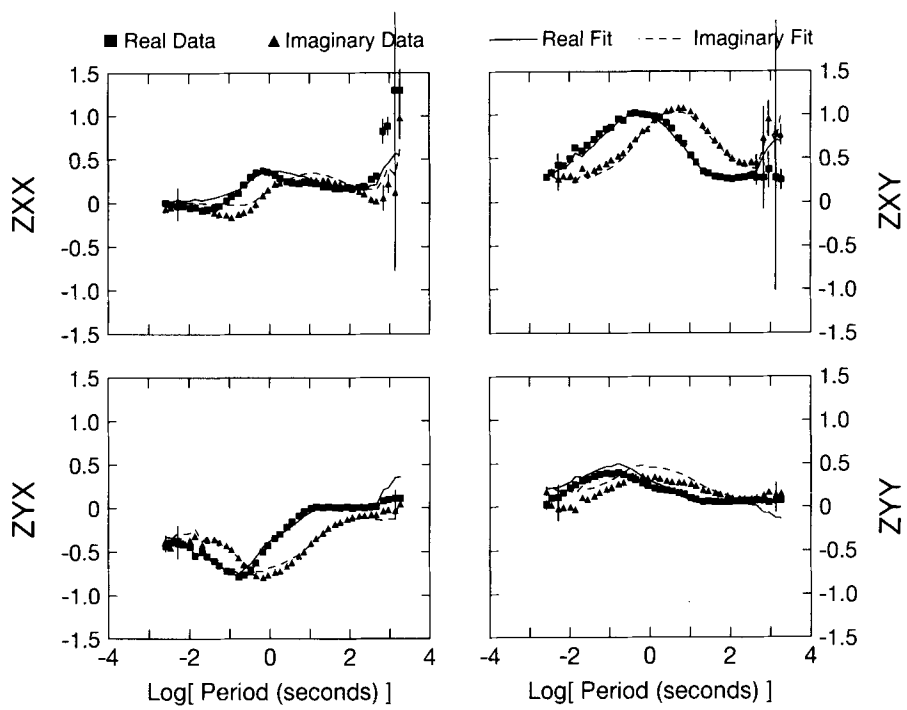

Figure 19(b). Fit to scaled impedance data.

azimuth swings towards 0°, the minor phase increases out of the first quadrant and the diagonal impedance elements (not shown) are poorly fit. The impedance tensor is essentially singular at long periods, for which GB2 have shown that the major 2-D impedance estimate is well determined, but the minor is not. GB2 also shows that phases increasing out of quadrant can be generated in synthetic data by strong 3-D effects on 2-D regional responses. If the strike is constrained to the short-period azimuth (Fig. 21), the minor phase is better behaved but the residual error is still large at longer periods. For 3-D electric distortions, 2-D models generally result in linear combinations of the 2-D regional responses which depend on the chosen strike. In this example, the choice of strike results in a minor phase similar to, but offset from, the major phase.

Figure 22 shows the unconstrained parameters for

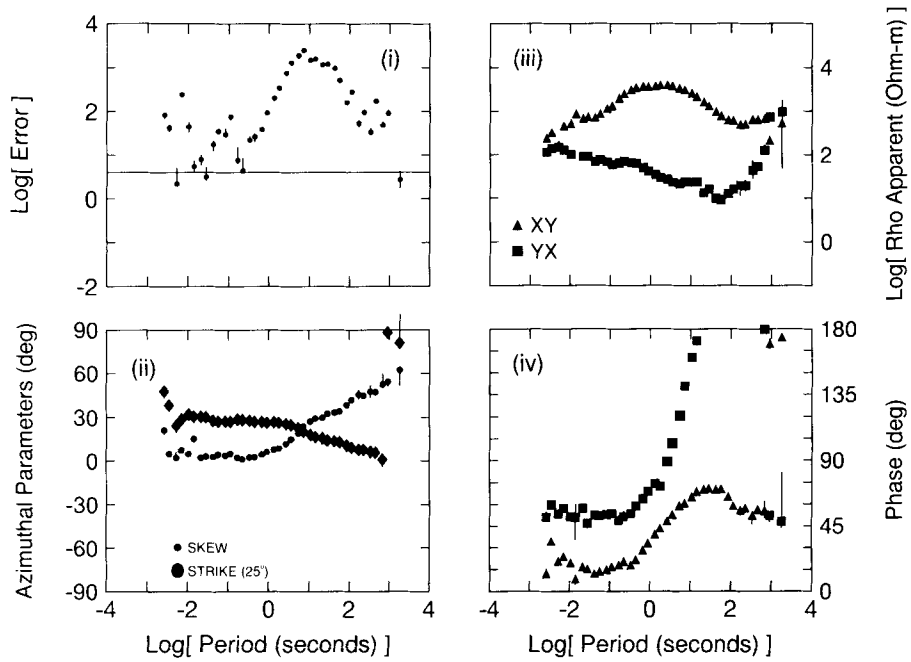

Figure 20. The 2-D model parameters for field data (LIT000) for best fitting strike.

parameterization model (3). The residual error is uniformly low. The short-period strike is about 30° with very small 3-D parameters as indicated by the previous 2-D parameterization model. As the skew increases with period, the 3-D parameters also increase dramatically with the shear approaching a value of 45°. This is a strong indication of impedance tensor singularity. The ramifications of this singularity can be studied with eq. (3b). The determinant of the estimated impedance tensor is the product of the determinants of its constituent tensors [i.e. **T**, **S**, **A** and $\mathbf{Z}_2$ (GB1)]. The rotation operators, including the twist operator, have determinants of one. A shear angle of 45° implies $|e| = 1$ (GB1) and accordingly the shear operator, and thus the total data tensor, have a determinant of zero (GB1). In such a case, inversion for model parameters can be a very unstable process with strong noise bias in a parameter estimate. This is particularly true for the strike, which was previously demonstrated to be a poorly constrained parameter in the presence of noise (Jones & Groom 1993).

Figure 23 shows the parameter variations for the 3-D

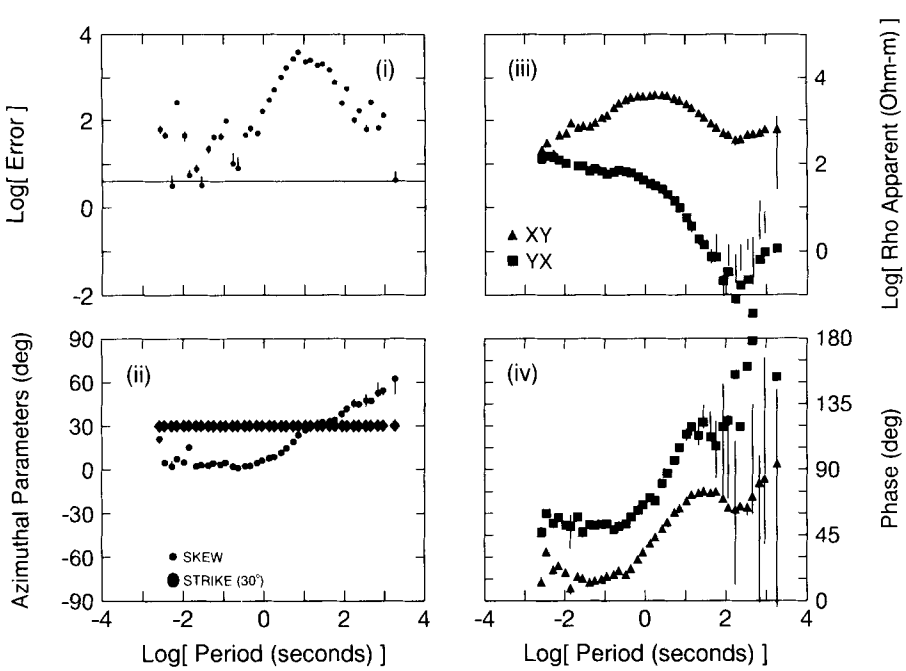

Figure 21. The 2-D model parameters for field data (LIT000) with strike constrained to short-period 2-D strike azimuth (30°).

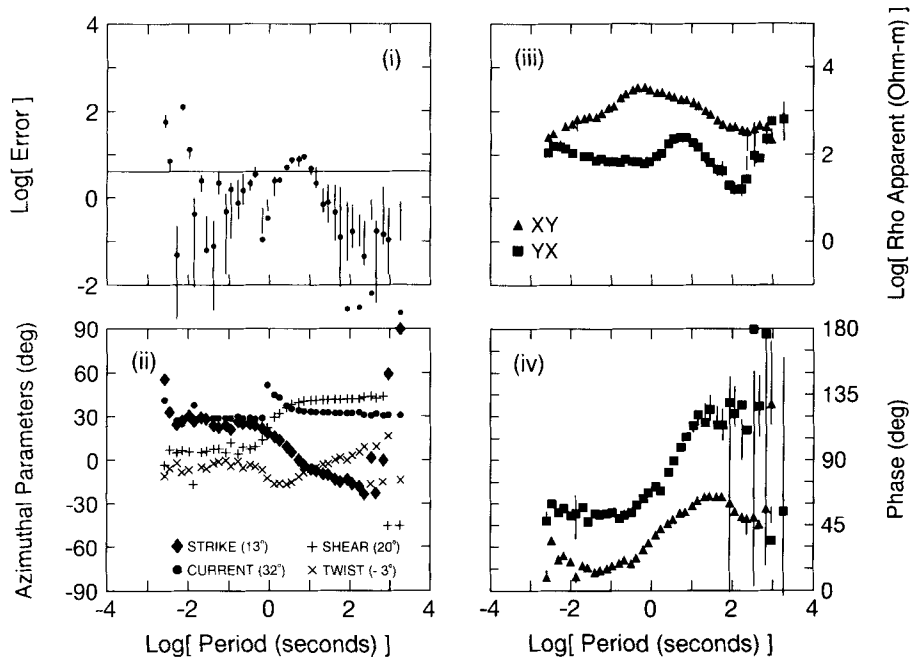

Figure 22. The unconstrained 3-D model parameters for field data (LIT000).

model as a function of period and regional strike. The residual error indicates that at short periods a 2-D model with very small static 3-D effects and with a strike azimuth of 25° to 30° parallel to the valley is the most appropriate. At about 1.0 s period the azimuth starts to swing towards 0°, an azimuth parallel to the western boundary of the Nelson batholith. In this mid-range, with the strike changing and with a transition from weak to strong distortion parameters (twist and shear), it is possible that model (3) will not fit the data adequately, since both 3-D inductive and 3-D galvanic magnetic effects are expected. These 3-D effects are frequency dependent, however, and should fall off as $\sqrt{\omega}$ (GB2). Model (3) should be adequate again by 10 s period. At the longer periods the strike azimuth approaches 60° but is not well determined. The channelling azimuth (lower right panel, Fig. 23) indicates that the current remains constrained to flow at 25° to 30°, parallel to the valley at all periods. Since the shear is relatively uniform and the twist is

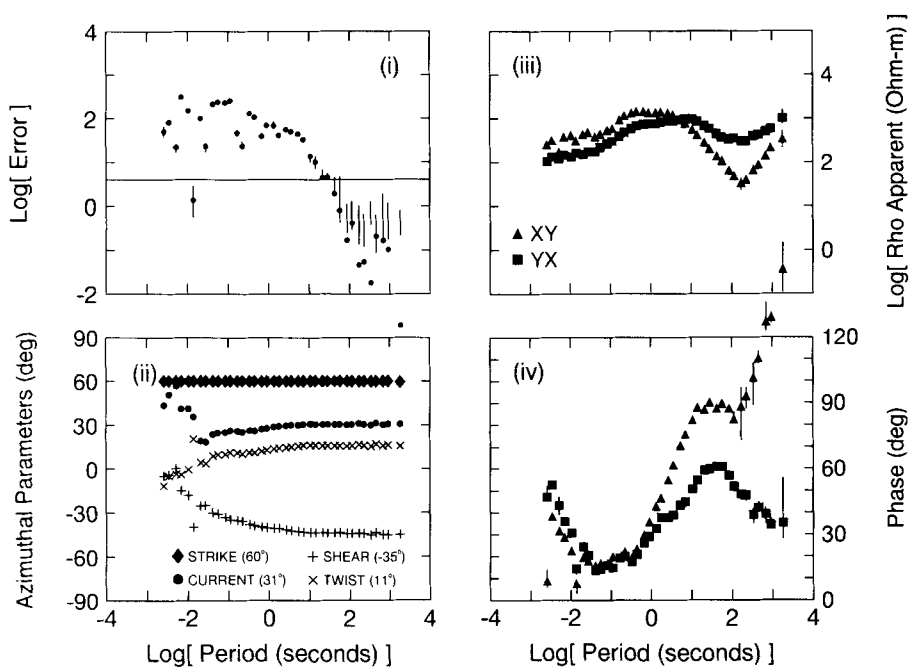

Figure 24. The 3-D model azimuthal parameters and residual for field data (LIT000) for strike constrained to 60°

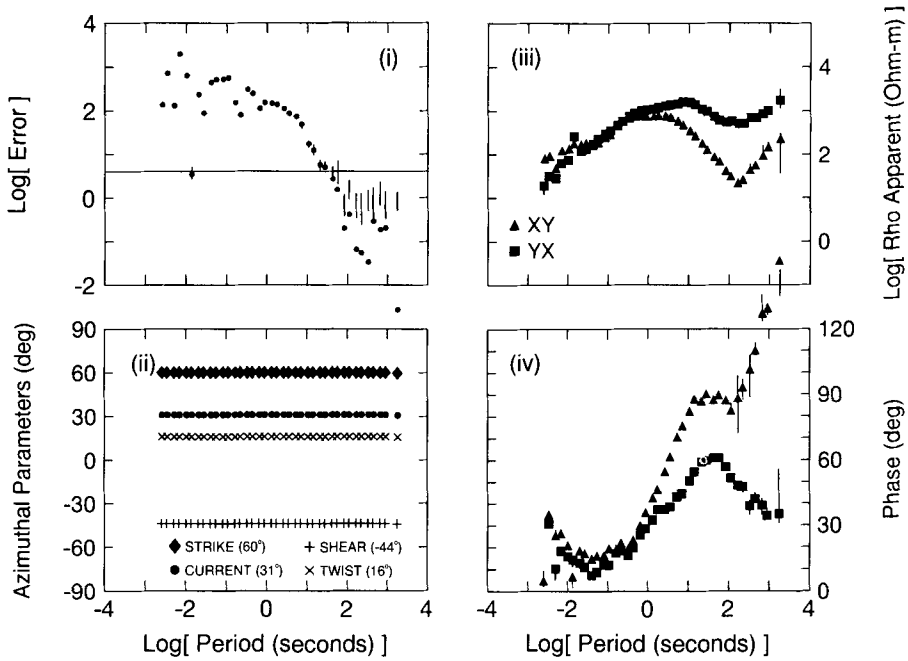

Figure 25. Final model parameters after correction for anisotropy in apparent resistivities for site LIT000.

frequency independent for most strike angles, and since the tensor is nearly singular at long periods, information from other sites is required to fix the strike. Fig. 24 shows the decomposition azimuthal and error results with unconstrained distortion parameter but with the regional strike constrained to 60° as suggested by Fig. 23, and the analyses of site LITW02. This azimuth is adequate for the regional strike for periods longer than 1 s as evidenced by the residual error (Fig. 24[i]), and by the constant distortion parameters. The current polarization azimuth remains fixed around 30°. The short-period error arises almost entirely from misfitting the imaginary part of the Z_{xy} and Z_{yy} components of the data until 1 s (not shown), indicating possible 3-D source effects. Further constraining the model, with the distortion parameters fixed at the long-period mean values, results in the parameters and fit of Fig. 25. Again for periods longer than 1 s, there is a generally good fit to the data with some significant but not extreme misfit at shorter periods. Impedance estimates include removal of local anisotropy with $s \approx 0.19$.

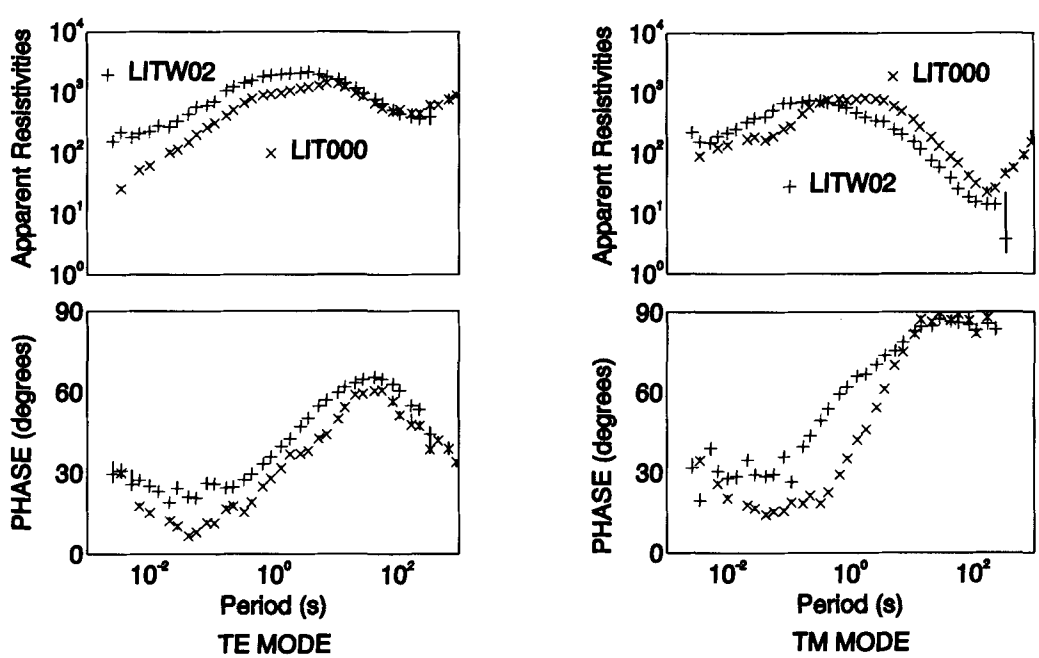

Figure 26. Comparison of recovered regional TE and TM mode responses after anisotropy corrections for stations LITW02 and LIT000.

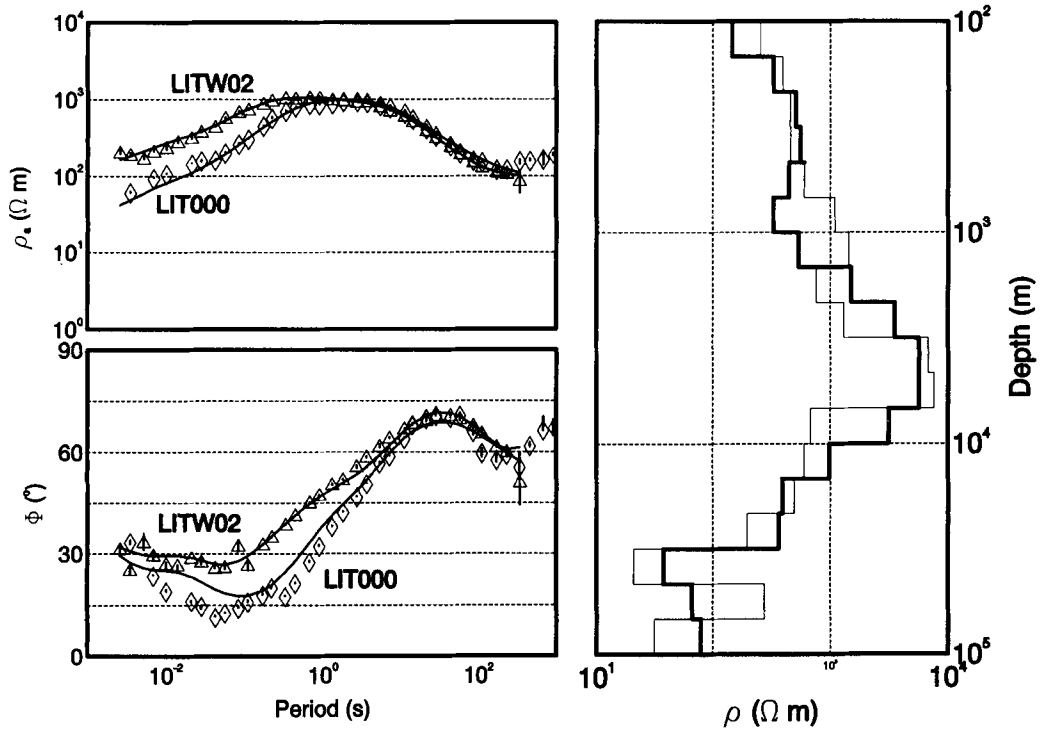

Figure 27. DTA estimators for stations LITW02 (bold response and model lines) and LIT000 with smooth minimum-structure inverses.

Regional responses for LIT000 and LITW02

Figure 26 shows a comparison of the regional estimates of apparent resistivity and phase from the final 3-D decomposition models and includes the anisotropy correction. The TE impedance corresponds to the Z_{yx} (Figs 18 and 25) component in the rotated decomposition model coordinate system. The TE impedance is assumed (with some evidence) to be parallel (N30°W) to the large-scale regional trends of the Cordillera and orthogonal to the present-day tectonic stress (Cook *et al.* 1988; Adams 1989). In addition, the shapes of the apparent resistivity curves at the long periods (Fig. 26) are characteristic of TM and TE responses observed at other stations in the survey. The similarity of the longer period regional phase responses from the two sites is quite remarkable when compared with phase estimates obtained by standard 2-D decomposition techniques. The TE mode apparent resitivities from the two sites are equivalent at longer periods. while the TM mode resistivities are parallel but slighly shifted from each other. This may be caused by different 2-D level effects (static shift) which would be expected from two separated sites or by an incorrect estimation of the local anisotropy or the final site gain (g) which may still be present.

The geological significance of the resulting impedance estimates becomes evident with the analyses of the entire suite of sites from the region. The results confirmed that the long-period phases recovered from the decomposition were indeed regional responses (Groom & Bahr 1992). The deep structural electrical anisotopy indicated in Fig. 26 is confirmed across the entire region (Jones *et al.* 1993).

Finally, Fig. 27 presents a comparison of the Decomposition Trace (DTA) apparent resistivity and phase data for the two sites. The short-period responses are different but they are almost identical at the longer periods as would be expected from two such closely spaced sites. The 1-D models (Fig. 27) were obtained using the minimum-structure inversion procedure of Constable *et al.* (1987). Parker's (1980) D^+ test provided the smallest misfit value possible for a 1-D model for both sites. The misfit values were increased by approximately 10 per cent to establish the minimum misfit allowed for the inversion. Both inversions give similar deeper crustal structures as was expected.

METHODOLOGY SYNOPSIS

From the above, it is clear that 3-D galvanic distortions can seriously affect MT data and lead to inappropriate strike angles being chosen which may result in erroneous interpretations. We have described a methodology for dealing with such distortions under a model of 3-D/2-D, i.e. 3-D distortion over a 2-D regional earth model. It is clear that for the case of 3-D/3-D our methodology is inappropriate. However, the frequency band of the inductive response of a body is normally quite small, compared to the bandwidth of modern MT systems (typically more than five decades), and thus often 3-D/3-D quickly becomes 3-D/2-D or 3-D/1-D with increasing period. Our proposed methodology to assess the dimensionality of the data, and to remove the distortions caused by local 3-D effects, can be summarized as follows.

(1) Test the rotational invariance of **Z**, thus fitting the data to a 1-D parameterization (1). The misfit to that model ($\log \gamma^2$, eq. 4) is then determined and if 95 per cent of the

misfit values lie below 4, then this 1-D model fits the data and no further analysis is appropriate or required. If the misfits are significantly above 4, then either the 1-D model is inappropriate, or the statistics of the data errors are too small. In either case, we go the step 2.1.

(2.1) Fit the data to a $5N$ free-parameter 2-D model (2) (i.e. frequency-dependent strike), and determine the misfit of this model. The definition of strike angle can be either from the data themselves, e.g. the Swift angle, or from other information, e.g. predominant geological strike of the region. If 95 per cent of the misfit values lie below 4, the next step is to try to find the appropriate strike direction for the entire frequency range of the data (step 2.2). If most values are above 4, then either the 2-D model is inappropriate, or the statistics of the data errors are too small. If the 2-D model has significantly lower misfits than the 1-D model, then we investigate whether a 3-D model has a lower misfit (step 3.1). If the misfit level has not decreased much with the 2-D model over the 1-D model, then we attempt to reduce any 3-D distortions with the model of 3-D over 1-D.

(2.2) Constrain the strike direction to that most consistent with much of the data. Determine the misfit for this model with $4N+1$ degrees of freedom (2-D with frequency-independent strike), and, if satisfactory (still below 4) then stop. Otherwise, go to step 2.3.

(2.3) A frequency-dependent 2-D strike implies that there are large bodies striking in different directions at different depths in the crust. In this situation the structure may be true 2-D at high frequencies, but then if 2-D/2-D at longer periods, a 2-D local distortion of a 2-D regional structure is produced. In this case, only the highest frequencies can be treated as true 2-D; for treating the data at longer periods, step 3.1 is required.

(3.1a) Perform an unconstrained fit of model (3) to the data over the whole bandwidth and inspect the misfits. Is the 3-D fit significantly better than the 2-D fit? If yes, go to step 3.1b. If not, then either the model of 3-D/2-D is inappropriate and the data are too sensitive to 3-D inductive effects, or a 2-D model is sufficient (go to 2.2).

(3.1b) Perform a strike-constrained fit varying the strike angle in increments between 0° and 90° and consider how the error and telluric distortion parameters vary, e.g. Figs 5, 8, 17 and 23. Is there a stable azimuth for which the distortion parameters are frequency independent and for which the error is minimized? If so, then one can be confident that the 3-D/2-D model is appropriate over the whole range of frequencies, and that one can continue with the analysis (go to step 3.2.). If not, then the anomalies are such that 3-D inductive effects are important for some part of the bandwidth, if not all. In this situation work from the surface downwards, i.e. from the highest frequencies to the lowest, until the 3-D/2-D model becomes inappropriate.

(3.2) Constrain the stablest of the telluric distortion or regional azimuthal parameters to a particular value or a small range of values over the whole bandwidth. In our experience either the *shear* or *twist* are far more stable than the regional rotation angle θ. This may not be possible over the entire bandwidth, in which case, treat the data in bands which are as broad as possible. In rare cases, the plot produced by step 3.1b will indicate that the regional strike is reasonably robust and well resolved. Then the strike angle should be constrained first because this will stabilize the non-linear estimation process for determining the telluric distortion parameters. It is possible that as the period increases, additional 3-D effects are significant. In which case, band-limited frequency-independent telluric distortion parameters are required.

(3.3) Constrain the second telluric distortion parameter; either the *twist* or *shear* depending on what was constrained in step 3.2.

(3.4) Constrain the strike angle θ to an angle which is most consistent over a broad band of frequencies and over as many sites as possible.

(3.5) It is necessary at this stage to ensure that the strike angle is appropriate for the data, and not one obtained by inappropriate choices of twist and shear. Accordingly, constrain the strike angle and permit the twist and shear to vary with frequency. Do they exhibit the originally constrained values? With some badly distorted, or noisy, data one must iterate between constraining the parameters in turn until a satisfactory model is determined.

(3.6) Remove the anisotropy. This can be done by determining the arithmetic mean of Z_{xy} and Z_{yx} at sufficiently high frequencies and shifting the two apparent resistivity curves to those levels.

The final correction which must be applied at each site is the local *site gain, g*, which is the same factor for both modes. This factor must be determined from other information, such as controlled-source soundings or from making assumptions about certain parts of the earth model, e.g. a uniform layer in the section (see Groom & Bahr 1992, and references therein).

CONCLUSIONS

In this paper we have described a systematic method for determining the appropriate dimensionality of MT data from a site, and we have illustrated the application of this method to analyse both synthetic data and real data. In addition, we described the extraction of regional impedance responses from multiple sites.

Synthetic studies have provided insight into the different physical parameterizations and parameter stability. In difficult cases, such as the field examples here, multiple sites need to be used to help constrain parameters. These parameters can then be used for modelling and inversion studies. Here we have demonstrated for two neighbouring sites that the analyses methodology can be extremely useful in unravelling the bulk regional response when hidden by strong 3-D effects.

As predicted by earlier theoretical work, the method applied to experimental data clearly indicated, as illustrated here with two sample sites, a result of significant geological importance which was not evident by standard techniques (Figs 15a and 20). Analyses of more than 20 sites have confirmed the general nature of the recovered regional response from the two sample sites, indicating electrical anisotropy deep in the crust (Jones *et al.* 1993). Although there may still be some uncertainties remaining in the true levels for the regional responses for stations LIT000 and LITW02, the analysis has provided models which not only fit the data but are consistent for neighbouring sites, whereas,

these data would initially suggest that the stations are seeing significantly different structures.

ACKNOWLEDGMENTS

We wish to acknowledge several people for their contributions to this paper. Dick Bailey for many fruitful discussions and his original decomposition concepts; Karsten Bahr for his insightful review and criticisms; Steve Constable for providing the Occam inversion code; Jim Craven and Toivo Korja for their comments on early drafts; Donnamaria DeCaires-Groom for proof reading the submitted copy; The Geological Survey of Canada for providing a Visiting Fellowship to RWG; Francois Richard for his careful and patient work in getting the decomposition processing software user-friendly; and Phoenix Geophysics (Toronto) Ltd for acquiring the field data discussed. Geological Survey of Canada Contribution No 14692.

REFERENCES

Adams, J. 1989. Crustal stresses in Eastern Canada, in *Earthquakes at North-Atlantic Passive Margins: Neotectonics and Postglacial Rebound*, pp. 289–297, eds Gregersen, S. & Basham, P. W., Kluwer Academic Publications, Dordrecht.

Bahr, K., 1988. Interpretation of the magnetotelluric impedance tensor: regional induction and local telluric distortion, *J. Geophys.*, **62,** 119–127.

Bahr, K., 1991. Geological noise in magnetotelluric data: a classification of distortion types, *Phys. Earth. planet. Inter.*, **66,** 24–38.

Berdichevsky, M. N. & Dmitriev, V. I., 1976. Basic principles of interpretation of magnetotelluric curves, in *Geolectric and geothermal studies*, pp. 165–221, ed. Adam, A., Akademini Kiado, Budapest, Hungary.

Cagniard, L., 1953. Basic theory of the magnetotelluric method of geophysical prospecting, *Geophysics*, **18,** 605–635.

Constable, S. C., Parker, R. L. & Constable, C. G., 1987. Occam's inversion: a practical algorithm for generating models from electromagnetic sounding data, *Geophysics*, **52,** 289–300.

Chakridi, R., Chouteau, M. & Mareschal, M., 1992. A simple technique for analysing and partly removing galvanic distortion from the magnetotelluric impedance tensor: application to Abitibi and Kapuskasing data (Canada), *Geophys. J. Int.*, **108,** 917–929.

Cook, F. A., Green, A. G., Simony, P. S., Price, R. A., Parrish, R. R., Milkereit, B., Gordy, P. L., Brown, R. L., Coflin, K. C. & Patenaude, C., 1988. Lithoprobe seismic reflection structure of the southeastern Canadian Cordillera: initial results, *Tectonics*, **67,** 157–180.

Groom, R. W., 1988. The Effects of Inhomogeneities on Magnetotellurics, *PhD thesis*, University of Toronto, Canada.

Groom, R. W. & Bahr, K, 1992. Corrections for near-surface effects: decomposition of the magnetotelluric impedance tensor and scaling corrections for regional resistivities, *Surv. Geophys.*, **13,** 341–380.

Groom, R. W. & Bailey, R. C., 1989. Decomposition of magnetotelluric impedance tensors in the presence of local three-dimensional galvanic distortion, *J. geophys. Res.*, **94,** 1913–1925.

Groom, R. W. & Bailey, R. C., 1991. Analytic investigations on the effects of near-surface three-dimensional galvanic scatterers on MT tensor decompositions, *Geophysics*, **56,** 496–518.

Jones, A. G., 1983. The problem of current channelling: a critical review, *Geophys. Surv.*, **6,** 79–122.

Jones, A. G. & Groom, R. W., 1993. Strike-angle determination from the magnetotelluric impedance tensor in the presence of noise and local distortion: rotate at your peril!, *Geophys. J. Int.*, **113,** 524–534.

Jones, A. G., Groom, R. W. & Kurtz, R. D., 1993. Decomposition and modelling of the BC87 dataset, *J. geomagn. Geoelect.*, in press.

Jones, A. G., Kurtz, R. D., Oldenburg, D. W., Boerner, D. E. & Ellis, R., 1988. Magnetotelluric observations along the Lithoprobe southeastern Canadian cordilleran transect, *Geophys. Res. Lett.*, **15,** 677–680.

Larsen, J. C., 1977. Removal of local surface conductivity effects from low frequency mantle response curves, *Acta Geodaet. Geophys. Montanist. Acad. Sci. Hung.*, **12,** 183–186.

Parker, R., 1980. The inverse problem of electromagnetic induction: existence and construction of solutions based on incomplete data, *J. geophys. Res.*, **35,** 4421–4425.

Pellerin, L. & Hohmann, G. W., 1990. Transient electromagnetic inversions: a remedy for magnetotelluric static shifts, *Geophysics*, **59,** 1242–1250.

Swift, C. M., Jr., 1967. A magnetotelluric investigation of an electrical conductivity anomaly in the southwestern United States, *PhD thesis*, MIT, Cambridge, MA.

Torres-Verdin, C. & Bostick, F. X., 1992. Principles of spatial surficial electric field filtering in magnetotellurics: electromagnetic array profiling (EMAP), *Geophysics*, **57,** 603–662.

Zhang, P., Roberts, R. G. & Pedersen, L. B., 1987. Magnetotelluric strike rules, *Geophysics*, **51,** 267–278.